

Pre-inflationary universe in loop quantum cosmology

Tao Zhu, Anzhong Wang

*Institute for Advanced Physics & Mathematics, Zhejiang University of Technology, Hangzhou, 310032, China
GCAP-CASPER, Physics Department, Baylor University, Waco, TX 76798-7316, USA*

Gerald Cleaver

EUCOS-CASPER, Physics Department, Baylor University, Waco, TX 76798-7316, USA

Klaus Kirsten and Qin Sheng

GCAP-CASPER, Mathematics Department, Baylor University, Waco, TX 76798-7328, USA

(Dated: October 25, 2017)

The evolutions of the flat FLRW universe and its linear perturbations are studied systematically in the dressed metric approach of LQC. When it is dominated by the kinetic energy of the inflaton at the quantum bounce, the evolution of the background can be divided into three different phases prior to the preheating, *bouncing, transition and slow-roll inflation*. During the bouncing phase, the evolution is independent of not only the initial conditions, but also the inflationary potentials. In particular, the expansion factor can be well described by the same exact solution in all the cases considered. In contrast, in the potential dominated case such a universality is lost. It is because of this universality that the linear perturbations are also independent of the inflationary models and obtained exactly. During the transition phase, the evolutions of the background and its linear perturbations are found explicitly, and then matched to the ones given in the other two phases. Hence, once the initial conditions are imposed, the linear scalar and tensor perturbations will be uniquely determined. Considering two different sets of initial conditions, one imposed during the contracting phase and the other at the bounce, we calculate the Bogoliubov coefficients and find that the two sets yield the same results and all lead to particle creations at the onset of the inflation. Due to the pre-inflationary dynamics, the scalar and tensor power spectra become scale-dependent. Comparing with the Planck 2015 data, we find constraints on the total e-folds that the universe must have expanded since the bounce, in order to be consistent with current observations.

I. INTRODUCTION

The inflationary paradigm not only solves elegantly the problems of the standard big bang cosmology, but also predicts the primordial power spectra whose evolutions determine the temperature fluctuations in cosmic microwave background (CMB) and the formation of the large-scale structure of the universe [1–3] (see [4] for an updated review). This prediction explains the power spectrum of the galaxy distribution, and has been remarkably confirmed by CMB measurements with unprecedented precisions [5–7].

However, the inflationary scenario is sensitive to the ultraviolet (UV) physics, and its successes are tightly contingent on the understanding of such UV physics [4]. In particular, the underlying quantum field theory on a classical spacetime becomes questionable for a large class of inflationary models, in which the e-folds of the expansion of the universe are more than 70 [8]. This is because in these models the sizes of the current universe are less than that of Planck at the onset of inflation, then the treatment of the spacetime as classical becomes invalid. This is the well-known trans-Planckian problem [9, 10]. In addition, general relativity (GR) inevitably leads to an initial singularity [11, 12], with which it is not clear how to impose the initial conditions. Instead, one usually ignores the pre-inflationary dynamics and sets the Bunch-Davies (BD) vacuum at the time when the pertur-

bation modes are inside the Hubble horizon during inflation. However, from the beginning of inflation (which is normally believed to start at the energy scale about 10^{16} GeV) to the Planckian scale, an energy gap of at least three-order exists. Once this pre-inflationary dynamics is taken into account, it is not clear how such a picture will be altered, as it is quite reasonable to expect that particles are created generically during the pre-inflationary phases, and non-BD states could be created even when the modes were well inside the Hubble horizon during inflation.

To address these important issues, loop quantum cosmology (LQC) provides an interesting framework, in which the big bang singularity is simply replaced by a quantum bounce in the deep Planck era, due to the quantum gravitational effects [13, 14], and a large number of cosmological models has been investigated [15–37], including the flat Friedmann-Lemaître-Robertson-Walker (FLRW) universe, the model that we shall focus on in this paper. In such a framework, the universe that was dominated by the kinetic energy of the inflaton at the bounce can eventually evolve to the desired slow-roll inflation [38–46].

An important question now is whether the quantum bounce and its subsequent pre-inflationary dynamics can leave any observational signatures to the current and/or forthcoming experiments, so LQC can be placed directly under tests. Such considerations have attracted a great deal of attention lately, see, for example, the special is-

sue of International Journal of Modern Physics D on *Loop Quantum Cosmology* [47], and the monograph of World Scientific, *Loop Quantum Gravity: The First 30 Years* [48]. A crucial step for connecting the quantum bounce with observations is the understanding of the evolutions of the background as well as the cosmological perturbations during the pre-inflationary period. Extensive studies have been carried out, but mainly numerical [47, 48]. In this paper, one of our goals is to study the quantum bounce and its subsequent pre-inflationary dynamics *analytically*, with the hope that it will provide deeper insights into the physics involved.

The studies of the pre-inflationary dynamics in the framework of LQC have been carried out by following mainly two different approaches [49], *dressed metric* [15–18] and *deformed algebra* [19–24]¹. In the latter, with some reasonable assumptions and the choice of initial conditions, it has been already shown that the resulting cosmological perturbations are in conflict with current observations [53, 54]. In the former, among other things, it was argued that the pre-inflationary effects could produce a way to relieve the tension between the standard spectra obtained in GR and observations at large scales [55].

In this paper, we shall provide a systematical study of the effects of the quantum bounce and its subsequent pre-inflationary dynamics on the background evolution and primordial perturbations in the framework of the *dressed metric approach* [15–18]. Earlier works on the subjects are mainly numerical [16, 18, 30, 31, 55, 56], and often requires time and memory intensive computations by using high-performance computing, in order to explore the most interesting region of the parameter space [56]. Our purpose in this paper is two-fold: First, we shall carry out an *analytical* investigation on the evolutions of both the background of the universe and its linear scalar and tensor perturbations. Second, we shall focus mainly on universal properties of the evolutions during the pre-inflationary period. That is, properties that do not depend on the inflationary potentials, so that they hold for any inflationary models. This is tightly related to the previous results that the universe that was dominated at the quantum bounce by the kinetic energy of the inflaton will eventually evolve to a desired slow-roll inflation [38–45].

Based on the above observations, in this paper we shall mainly consider the models that are dominated at the quantum bounce by the kinetic energy of the inflaton. In particular, we shall show that under this assumption not only the evolution of the background of the universe is universal, but also the evolutions of its linear perturbations during the pre-inflationary period. We also study models that are dominated at the bounce by the potential of the inflaton, and show explicitly that such uni-

versalities are lost. In particular, the rest of the paper is organized as follows. In Sec. II and III, we present a detailed analysis of the background evolution first numerically (Sec. II) and then analytically (Sec. III), and show that *the evolution of the background is universal and independent of the form of the inflationary potentials, as long as it is dominated by the kinetic energy of the inflaton at the quantum bounce*. Based on the understanding of the background evolution, in Sec. IV we turn to study the cosmological scalar and tensor perturbations. In particular, we show that the effective potentials of the perturbations of both scalar and tensor can be mimicked very well by a Pöschl-Teller (PT) potential during the bouncing phase, whereby we obtain analytically the mode functions of the perturbations. In Sec. V, we consider two different sets of initial conditions for the cosmological perturbations, one is *the Bunch-Davies (BD) vacuum imposed at the contracting phase right before the quantum bounce*, and the other is *the fourth-order adiabatic vacuum state imposed at the bounce*. By using our analytical solution we show explicitly that the BD vacuum state imposed at the contracting phase reduces to the fourth-order adiabatic vacuum state at the bounce. In addition, with these initial conditions, we also derive explicitly the analytical expressions of primordial power spectra and discuss the associated bouncing and pre-inflationary effects. In Sec. VI, we perform the CosmoMC code to study cosmological constraints by using the Planck2015 data [7]. Our main conclusions and discussions are presented in Sec. VII. Two appendices are also included. Part of the results have been already reported in [57].

II. BACKGROUND EVOLUTION: NUMERICAL

In this section, let us begin to consider the evolution of the flat FLRW background coupled with a single scalar field ϕ , the inflaton, in the framework of LQC,

$$ds^2 = -dt^2 + a(t)\delta_{ij}dx^i dx^j, \quad (2.1)$$

where $a(t)$ is the cosmological scale factor with t being the cosmic time. In LQC, the FLRW spacetime can be quantized by using the canonical quantization framework of loop quantum gravity. The quantized background spacetime together with the scalar field ϕ , is described by a quantum state $\Psi_0(a, \phi)$ which is a complex function of the scale factor $a(t)$ and scalar field ϕ . The evolution of this quantum state is governed by the LQC quantum Hamiltonian constraint, and a remarkable feature is that it is nonsingular. Among many states $\Psi_0(a, \phi)$ in the LQC Hilbert space, one is in general interested in a state that is sharply peaked around a classical trajectory at late times, when the curvature of the Universe is well below the Planck scale and the classical GR is an excellent approximation [33–36]. Evolving this state by using the LQC quantum Hamiltonian constraint, it has been shown

¹ Other approaches, such as separate universe [50], hybrid models [51] and consistent histories [52], are still in their developments.

that it remains sharply peaked during the whole dynamical trajectory, even in the deep Planck era [34, 35]. As a result, the evolution of the peak of such states can be accurately described by an effective trajectory that governed by its effective equations.

These effective equations for a flat FLRW background has been derived in Refs. [58–60] (see also [37] for an alternative approach), from which the modified Friedmann equation takes the form

$$H^2 = \frac{8\pi}{3m_{\text{Pl}}^2} \rho \left(1 - \frac{\rho}{\rho_c} \right), \quad (2.2)$$

where $H \equiv \dot{a}/a$ denotes the Hubble parameter and the dot represents the derivative with respect to the cosmic time t , $m_{\text{Pl}} = 1/\sqrt{G}$ is the Planck mass, ρ is the energy density of the universe, and ρ_c is the critical energy density which represents the maximum value of the energy density in LQC and is about $\rho_c \simeq 0.41m_{\text{Pl}}^4$. For a single scalar field ϕ with a potential $V(\phi)$ in the FLRW background, the effective equation of motion in LQC takes the same form of the Klein-Gordon equation as in GR,

$$\ddot{\phi} + 3H\dot{\phi} + V_{,\phi} = 0, \quad (2.3)$$

where $V_{,\phi} = dV(\phi)/d\phi$.

A robust prediction of the above effective dynamics is the occurrence of a non-singular quantum bounce, which removed the initial singularity in the early stage of the classical universe (see [32–37] and references therein). Eq. (2.2) shows that the quantum bounce occurs at $\rho = \rho_c$, where the energy density reaches the maximum value and the Hubble parameter becomes zero. The background evolution with a bounce phase has been extensively studied, and one of the main results is that, right following the quantum bounce, a desired slow-roll inflation phase is almost inevitable [13, 40–43] (for recent considerations, see [55]).

It is remarkable to note that the modified Friedmann equation (2.2) and the Klein-Gordon equation (2.3) are also derived in *the deformed algebra approach* [19–24]. Hence, all the results obtained in this section as well as the results obtained in the next section will be equally applicable to this approach, too.

In this section, we will study the “bounce plus slow-roll inflation” scenario by considering two typical inflationary potentials, the power-law potential and Starobinsky potential, as specified below:

- *Inflation with a power-law potential.* A power-law potential takes the form

$$V(\phi) = \frac{1}{2} m^{4-n} \phi^n, \quad (2.4)$$

where the parameter m has dimension of mass. We consider two specific values of n : $n = 2$ and $n = 1/2$, respectively. The corresponding values of the mass for each potential used for numerical

calculations are set to

$$m = \begin{cases} 1.3 \times 10^{-6} m_{\text{Pl}}, & n = 2, \\ 7.4 \times 10^{-4} m_{\text{Pl}}, & n = \frac{1}{2}. \end{cases} \quad (2.5)$$

Note that these values are chosen to be consistent with Planck 2015 data [7].

- *R^2 -inflation.* This is also known as the Starobinsky inflation, whose potential has the form

$$V(\phi) = \frac{3}{32\pi} M^2 m_{\text{Pl}}^2 \left(1 - e^{-\sqrt{\frac{16\pi}{3}} \frac{\phi}{m_{\text{Pl}}}} \right)^2, \quad (2.6)$$

where the parameter M has dimension of mass, whose value used for numerical calculations is set to [7, 31]

$$M = 2.51 \times 10^{-6} m_{\text{Pl}}, \quad (2.7)$$

to be consistent with Planck 2015 data.

In this paper, we find that it is also convenient to use the conformal time,

$$\eta = \int_{t_{\text{end}}}^t \frac{dt'}{a(t')}, \quad (2.8)$$

so that at the end of the inflation $t = t_{\text{end}}$ and at the bounce t_{B} , the corresponding conformal times are, respectively, given by

$$\eta_{\text{end}} = 0, \quad \eta_{\text{B}} = \int_{t_{\text{end}}}^{t_{\text{B}}} \frac{dt'}{a(t')}. \quad (2.9)$$

Let us first study the background evolution numerically for different inflationary potentials. Eqs. (2.2) and (2.3) can be solved numerically by imposing the initial conditions for $a(t)$, $\phi(t)$, and $\dot{\phi}(t)$ at a specific point. A convenient choice of such a point is the bounce $t = t_{\text{B}}$, at which we have the relations

$$\frac{1}{2} \dot{\phi}^2(t_{\text{B}}) + V(\phi(t_{\text{B}})) = \rho_c, \quad \text{and} \quad \dot{a}(t_{\text{B}}) = 0. \quad (2.10)$$

Thus, if we consider ρ_c as a given constant, using the first equation we can write $\dot{\phi}_{\text{B}}$ in terms of ρ_c and ϕ_{B} , once a potential $V(\phi)$ is specified. Therefore, now we only need to specify $a(t_{\text{B}})$ and $\phi(t_{\text{B}})$ as the initial conditions. For the sake of simplicity, we further rescale $a(t)$ by setting $a(t_{\text{B}}) = 1$ at the bounce. Then, the initial conditions finally reduce to specifying the value of $\phi(t_{\text{B}})$ only. In the following, we shall consider the two classes $\dot{\phi}_{\text{B}} > 0$ and $\dot{\phi}_{\text{B}} < 0$, separately.

We shall pay particular attention to two important issues, namely how likely the occurrence of the slow-roll inflation is, and whether enough e -folds can be generated during the slow-roll inflation. For these purposes, let us first introduce the following background quantities:

- (1) The equation of state $w(\phi)$, which is defined by

$$w(\phi) \equiv \frac{\dot{\phi}^2/2 - V(\phi)}{\dot{\phi}^2/2 + V(\phi)}. \quad (2.11)$$

During the slow-roll inflation, $w(\phi)$ has to be very close to -1 .

- (2) The slow-roll parameter ϵ_H , which is defined by the derivative of the Hubble parameter,

$$\epsilon_H \equiv -\frac{\dot{H}}{H^2}. \quad (2.12)$$

During the slow-roll inflation, ϵ_H is required to be very small, i.e., $\epsilon_H \ll 1$.

- (3) The e -folds of the slow-roll inflation N_{inf} , which is defined as the e -folds between the onset of the slow-roll inflation until the end of it,

$$N_{\text{inf}} \equiv \ln \left(\frac{a_{\text{end}}}{a_i} \right). \quad (2.13)$$

In this paper, the onset of the inflation is defined by the time when the universe begins to accelerate, $\ddot{a}(t_i) = 0$, i.e., $\ddot{a}(t)$ first changes its sign right after the bouncing phase. The end of the inflation is defined by the time when the accelerating expansion of the universe stops, that is, $w(\phi_{\text{end}}) = -1/3$.

In the following, we shall study the background evolution for each of the two potentials mentioned above separately.

A. Quadratic potential

Let us begin by discussing the evolution of the background with the quadratic potential (i.e., Eq. (2.4) with $n = 2$), which has already been discussed in detail in Refs. [18, 56]. Here we summarize some main results.

As the initial conditions for the quadratic potential at the bounce have the symmetry $(\phi_B, \dot{\phi}_B) \rightarrow (-\phi_B, -\dot{\phi}_B)$, in this subsection we only need to consider the case $\dot{\phi}_B > 0$, and the results can be easily extended to the case $\dot{\phi}_B < 0$ by using the above symmetry. We can further divide the initial conditions into two subclasses, the kinetic energy dominated and the potential energy dominated cases at the quantum bounce.

The background evolution for a set of kinetic energy dominated initial conditions is illustrated in Fig. 1, in which the scale factor $a(t)$, the equation of state $w(\phi)$, and the slow-roll parameters ϵ_H are all obtained numerically for the same set of the initial values of ϕ_B . It is shown clearly that the desired slow-roll inflationary phase for these initial conditions is achieved. During this phase, the scale factor is exponentially growing (c.f. the top panel of Fig. 1), and $w(\phi)$ is very close to -1 (c.f.

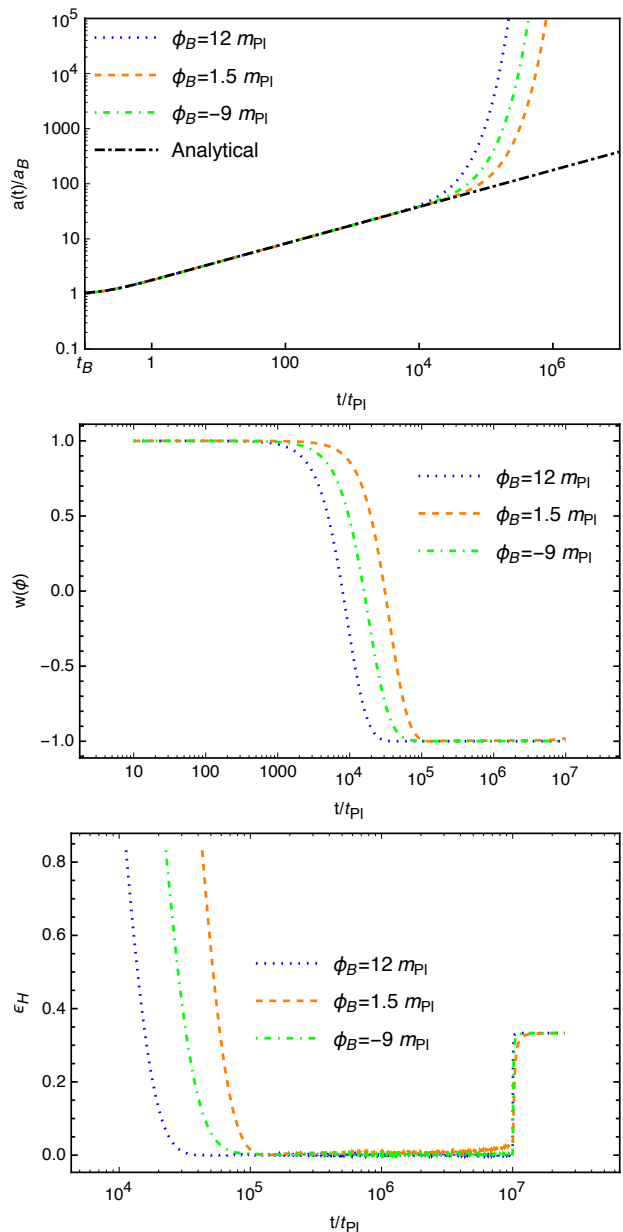


FIG. 1. Numerical solution for the quadratic potential with kinetic energy dominated initial conditions at the bounce and $\dot{\phi}_B > 0$. Top panel: the evolution of the scale factor $a(t)$ for different choices of the initial conditions. The analytical solution given by Eq. (3.4) is also shown in order to compare it with the numerical ones. Middle panel: the equation of state $w(\phi)$ for the same set of initial conditions. Bottom panel: the slow-roll parameter ϵ_H during the transition and slow-roll inflationary phases.

the middle panel of Fig. 1), while the parameter $\epsilon_H \ll 1$ (c.f. the bottom panel of Fig. 1). For initial conditions with $\dot{\phi}_B < 0$, the replacement ϕ_B by $-\phi_B$ [so that now $\phi_B/m_{\text{Pl}} \in (-12, -1.5, 9)$] shall yield the same results.

From the curves of the equation of state $w(\phi)$ [the middle panel of Fig. 1], we can see clearly that the evolu-

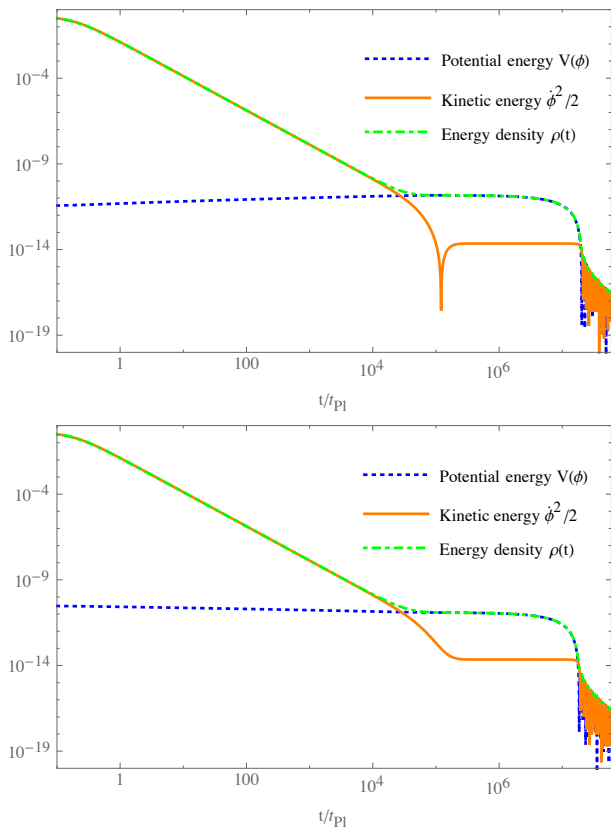


FIG. 2. Comparison between the potential energy $V(\phi)$ and the kinetic energy $\dot{\phi}^2/2$ for the quadratic potential. The energy density $\rho = \dot{\phi}^2/2 + V(\phi)$ is also shown. Top panel: for the initial condition $\phi_B = 2m_{\text{Pl}}$ with $\dot{\phi}_B > 0$. Bottom panel: for the initial condition $\phi_B = 6m_{\text{Pl}}$ with $\dot{\phi}_B < 0$.

tion of the universe before preheating can be divided into three different phases, *the bouncing, transition and slow-roll inflation*. During the bouncing phase, the kinetic energy of the inflaton is dominant, and $w(\phi) \simeq +1$. At $t/t_{\text{Pl}} \simeq 10^4$, $w(\phi)$ suddenly decreases from $w(\phi) \simeq +1$ to $w(\phi) \simeq -1$ at $t/t_{\text{Pl}} \simeq 10^5$. Comparing with the other two phases, this transition phase is rather short. Afterward, $w(\phi)$ remains $w(\phi) \simeq -1$ until the end of the slow-roll inflation. It is remarkable to note that the evolution of the expansion factor $a(t)$ during the bouncing phase is independent of the choices of the initial values of ϕ_B , and can be well described by the analytical solution given by Eq. (3.4) below.

In Fig. 2, the kinetic and potential energies, as well as the energy density of the inflationary field ϕ , are illustrated for both $\dot{\phi}_B > 0$ and $\dot{\phi}_B < 0$. A remarkable feature is that the potential energy remains almost the same during the three different phases, while the kinetic energy starts at about the Planckian energy at the bounce and then drops about 12-orders before the slow-roll inflation starts, whereby the potential energy starts to dominate the evolution of the universe.

The corresponding e-folds N_{inf} during the slow-roll in-

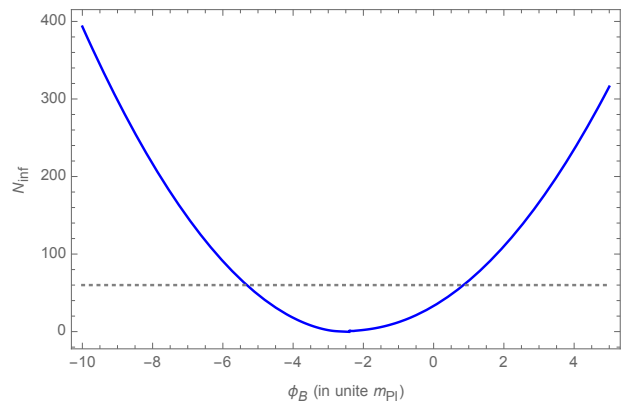


FIG. 3. The e-folds N_{inf} during the slow-roll inflationary phase for different choices of the initial condition ϕ_B for the case $\dot{\phi}_B > 0$. The gray dotted line represents the minimum value of e-folds ($N_* = 60$), in order to be consistent with observations.

flation as a function of ϕ_B is illustrated in Fig. 3. In order to produce at least 60 e-folds during the slow-roll inflation, Fig. 3 shows clearly that one has to require

$$\phi_B \in (-\phi_{\text{max}}, -5.3m_{\text{Pl}}) \cup (0.83m_{\text{Pl}}, \phi_{\text{max}}), \quad (2.14)$$

for $\dot{\phi}_B > 0$, where $\phi_{\text{max}} = \sqrt{2\rho_c/m}$. For the initial conditions with $\dot{\phi}_B < 0$, using the symmetry $(\phi_B, \dot{\phi}_B) \rightarrow (-\phi_B, -\dot{\phi}_B)$, one gets the constraints

$$\phi_B \in (-\phi_{\text{max}}, -0.83) \cup (5.3m_{\text{Pl}}, \phi_{\text{max}}). \quad (2.15)$$

The e-folds N_{inf} increases when the absolute values of ϕ_B is increasing, which implies that a larger value of the potential energy at the bounce can produce more e-folds during the slow-roll inflation than a smaller one. Note that similar results were already obtained in [18, 56].

When the potential energy $V(\phi)$ of the inflaton dominates at the quantum bounce, the background evolution of the universe is illustrated in Fig. 4, from which we can see that the universality of the evolution of $a(t)$ disappears. In fact, the bouncing phase does not exist any more, although the slow-roll inflationary phase $w(\phi) \simeq -1$ can be still achieved.

B. Power-law potential with $n = 1/2$

We continue considering the power-law potential in this subsection but now focus on $n = 1/2$, for which the value of the scalar field ϕ must be positive in order for the potential to be real. Similar to the quadratic potential case, we further divide the initial conditions into two subclasses, the kinetic energy dominated and the potential energy dominated.

Let us first consider the case in which the evolution is dominated at the bounce by the kinetic energy of the inflaton. Then, the background evolutions for a set of initial conditions with $\dot{\phi}_B > 0$ and $\dot{\phi}_B < 0$ are illustrated,

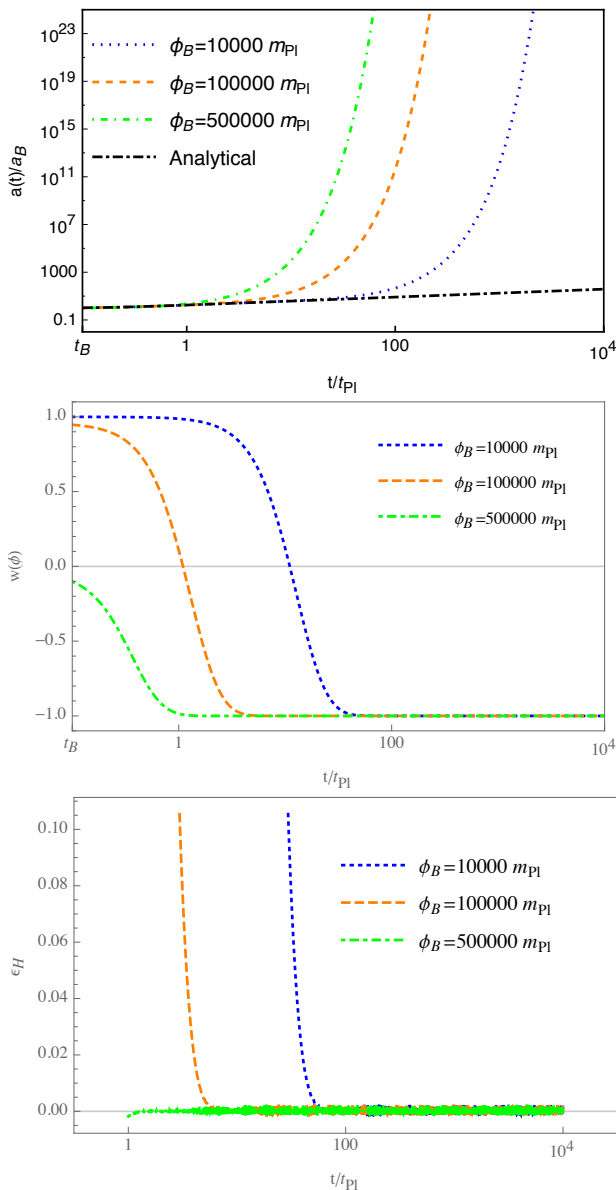


FIG. 4. Numerical solution for the quadratic potential with the initial condition that the potential energy dominates the evolution of the universe at the bounce for $\dot{\phi}_B > 0$. Top panel: the evolution of the scale factor $a(t)$. The analytical solution given by Eq. (3.4) is also illustrated. Middle panel: the equation of state $w(\phi)$ for the same set of initial conditions as those given in Top panel. Bottom panel: the slow-roll parameter ϵ_H .

respectively, in Fig. 5 and Fig. 6, in which the scale factor $a(t)$, the equation of state $w(\phi)$, and the slow-roll parameters ϵ_H are all obtained numerically. To see the universality of the evolution of the scale factor $a(t)$, its analytical solution of Eq. (3.4) is also illustrated. From these figures, we find that: (a) similar to the quadratic potential case, the evolution of the universe can be divided into three different phases, the bouncing, transition and slow-roll inflation. (b) During the bouncing phase,

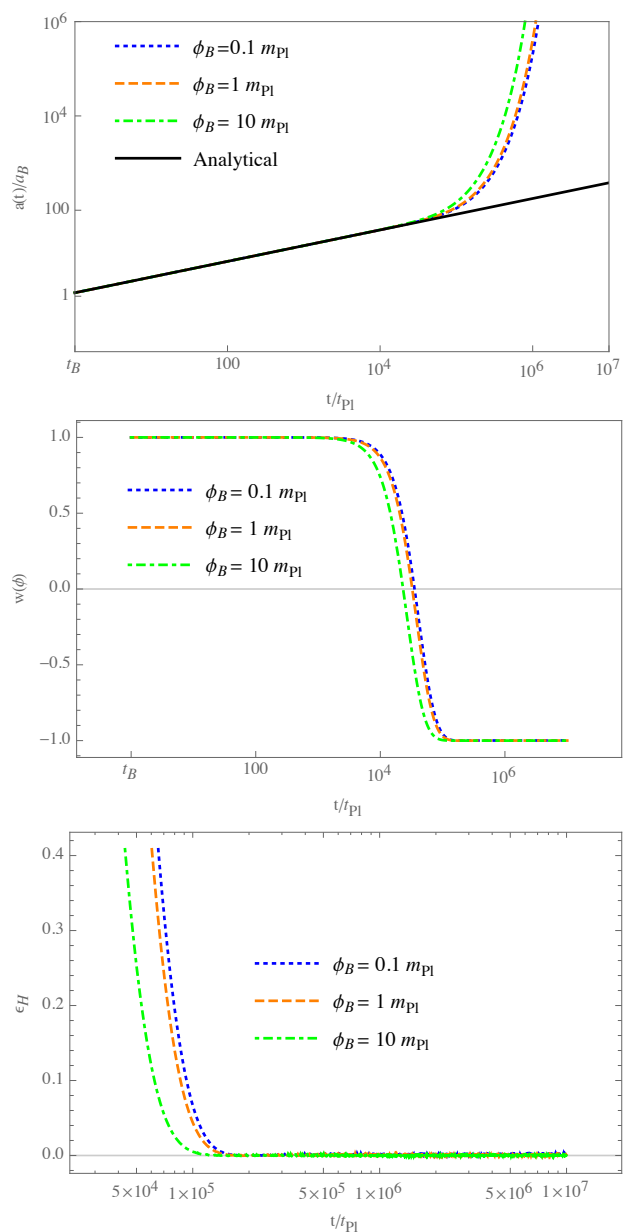


FIG. 5. Numerical solution for the power-law potential with $n = 1/2$ and the kinetic energy dominates the evolution at the bounce with $\dot{\phi}_B > 0$. Top panel: the evolution of the scale factor $a(t)$. The analytical solution given in Eq. (3.4) is also illustrated. Middle panel: the equation of state $w(\phi)$ with the same set of the initial conditions as those given in Top panel. Bottom panel: the slow-roll parameter ϵ_H .

the evolution of the scale factor $a(t)$ is independent of not only the initial conditions of ϕ_B and $\dot{\phi}_B$, but also the potential. It is well described by the analytical solution given by Eq. (3.4) for the quadratic potential ($n = 2$) as well as for the power-low potential with $n = 1/2$. In fact, as we shall show below, this is also true for the Starobinsky potential. This is mainly because the amplitude of the potential during the bouncing phase is very small in

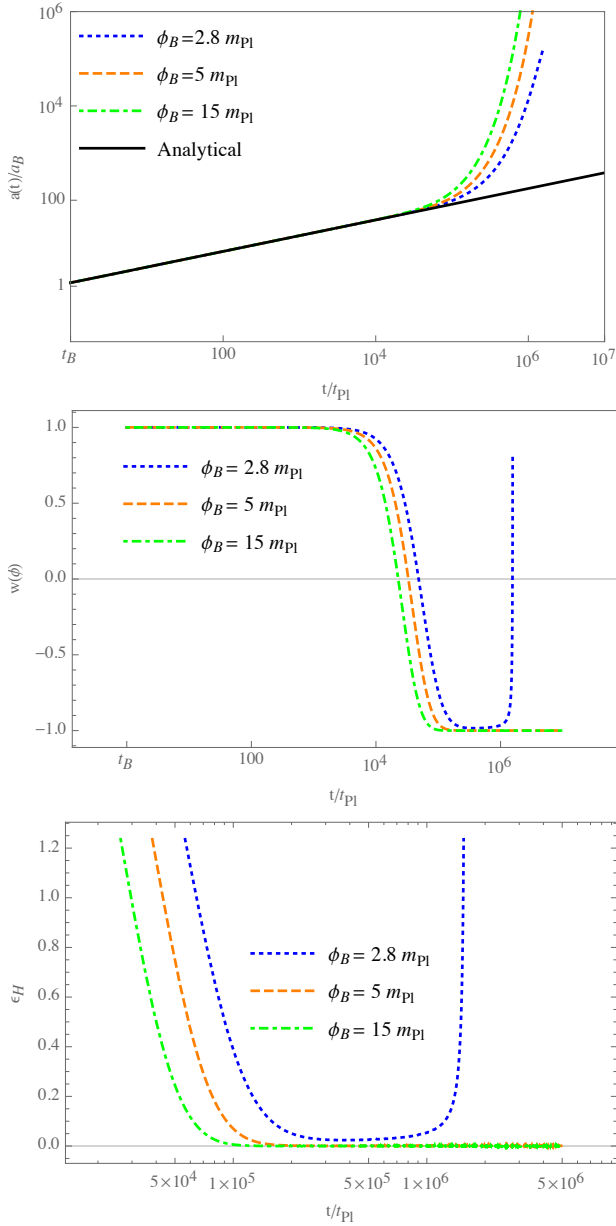


FIG. 6. Numerical solution for the power-law potential with $n = 1/2$ and the kinetic energy dominates the evolution at the bounce with $\dot{\phi}_B < 0$. Top panel: the evolution of the scale factor $a(t)$. The analytical solution given in Eq. (3.4) is also illustrated. Middle panel: the equation of state $w(\phi)$ for the same set of initial conditions as those in Top panel. Bottom panel: the slow-roll parameter ϵ_H .

comparison with the kinetic one, and its effects on the evolution of the background during the bouncing phase are negligible. This can be seen clearly from Fig. 2 for the quadratic potential and Fig. 7 for the power-law potential with $n = 1/2$.

The corresponding e-folds N_{inf} during the slow-roll inflation as a function of ϕ_B is illustrated in Fig. 8. For the initial conditions with $\dot{\phi}_B > 0$, the top panel of

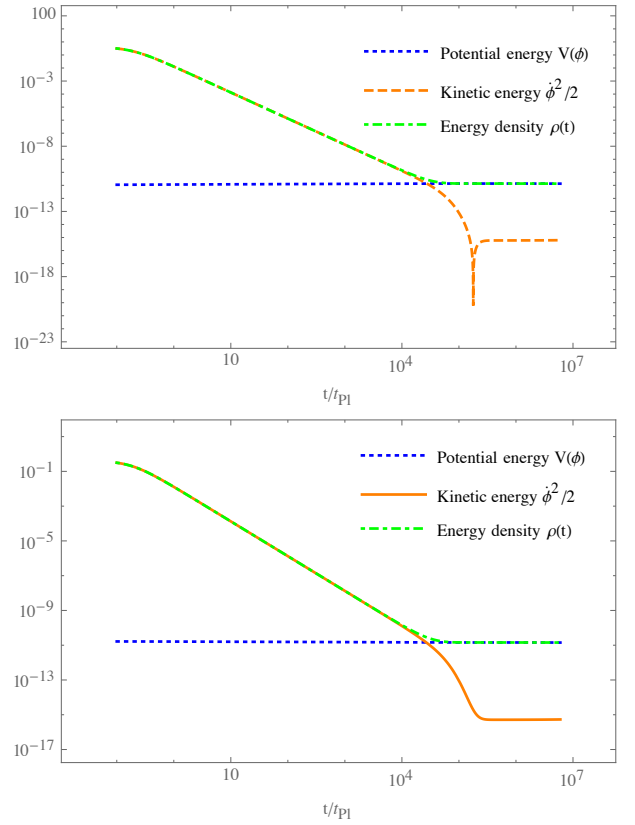


FIG. 7. Comparison between the potential energy $V(\phi)$ and the kinetic energy $\dot{\phi}^2/2$. The energy density $\rho = \dot{\phi}^2/2 + V(\phi)$ for the power law potential with $n = 1/2$ is also illustrated. Top panel: for the initial condition $\phi_B = 4m_{\text{Pl}}$ and $\dot{\phi}_B > 0$. Bottom panel: for the initial condition $\phi_B = 9m_{\text{Pl}}$ and $\dot{\phi}_B < 0$.

Fig. 8 shows that the desired slow-roll inflation can be produced for any value of ϕ_B in the range of $(0, \phi_{\text{max}})$. Here $\phi_{\text{max}} = \frac{4\rho_c^2}{m^2}$. Moreover, the slow-roll inflation can last long enough to produce more than 60 e-folds. For the initial conditions with $\dot{\phi}_B < 0$, in order to produce at least 60 e-folds during the slow-roll inflationary phase, the values of ϕ_B have to be restricted to

$$\phi_B \in [3.7m_{\text{Pl}}, \phi_{\text{max}}]. \quad (2.16)$$

Similar to the quadratic potential, the e-folds N_{inf} increases when the value of ϕ_B is increasing.

For the evolution in which the potential energy dominates at the quantum bounce, the background evolution is presented in Fig. 9. Again, in this case the evolution of the scale factor sensitively depends on the choice of the initial conditions of ϕ_B and $\dot{\phi}_B$. But, the slow-roll inflation is still achieved, and similar to the quadratic potential, the potential energy dominated initial conditions can lead to a large number of e-folds N_{inf} during the slow-roll inflation.

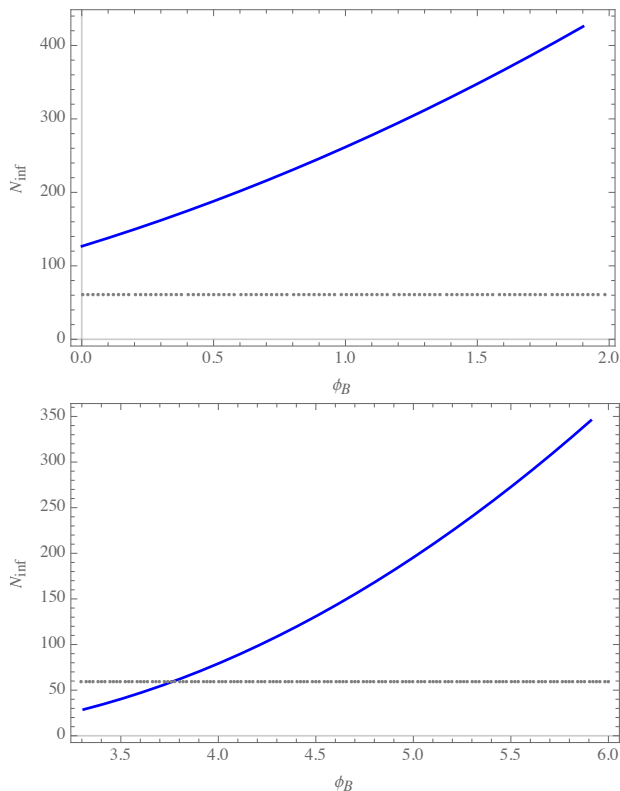


FIG. 8. The e-folds N_{inf} during the slow-roll inflation as a function of ϕ_B for the power-law potential with $n = 1/2$. Top panel: for $\dot{\phi}_B > 0$. Bottom panel: for $\dot{\phi}_B < 0$.

C. Starobinsky potential

The behavior of the background evolution with the Starobinsky potential has been studied in detail in [30, 31]. Here we again summarize some of their main results, by paying particular attention on the universal properties.

The potential energy of the scalar field cannot exceed the maximum value ρ_c , so that the value of ϕ_B can only lie in the range of $(\phi_{\text{min}}, +\infty)$, where

$$\phi_{\text{min}} = -\frac{\sqrt{3}m_{\text{Pl}}}{4\sqrt{\pi}} \ln \left(1 + \frac{\sqrt{32\pi\rho_c}}{\sqrt{3}Mm_{\text{Pl}}} \right). \quad (2.17)$$

For the value of M given by Eq. (2.7) (see Ref. [31] for details), we have $\phi_{\text{min}} = -3.47m_{\text{Pl}}$, and the potential energy can dominate the evolution only in a very narrow range $\phi \in [\phi_{\text{min}}, -3m_{\text{Pl}})$. In order to identify what kind of initial conditions can lead to sufficiently long slow-roll inflation, we search all the parameter space of ϕ numerically.

The results of the background evolutions for the kinetic energy dominated initial conditions are illustrated in Fig. 10 and Fig. 11, with $\dot{\phi}_B > 0$ and $\dot{\phi}_B < 0$, respectively. In both figures, the scale factor $a(t)$, the equation of state $w(\phi)$, and the slow-roll parameters ϵ_H are all obtained numerically for the same set of initial values of

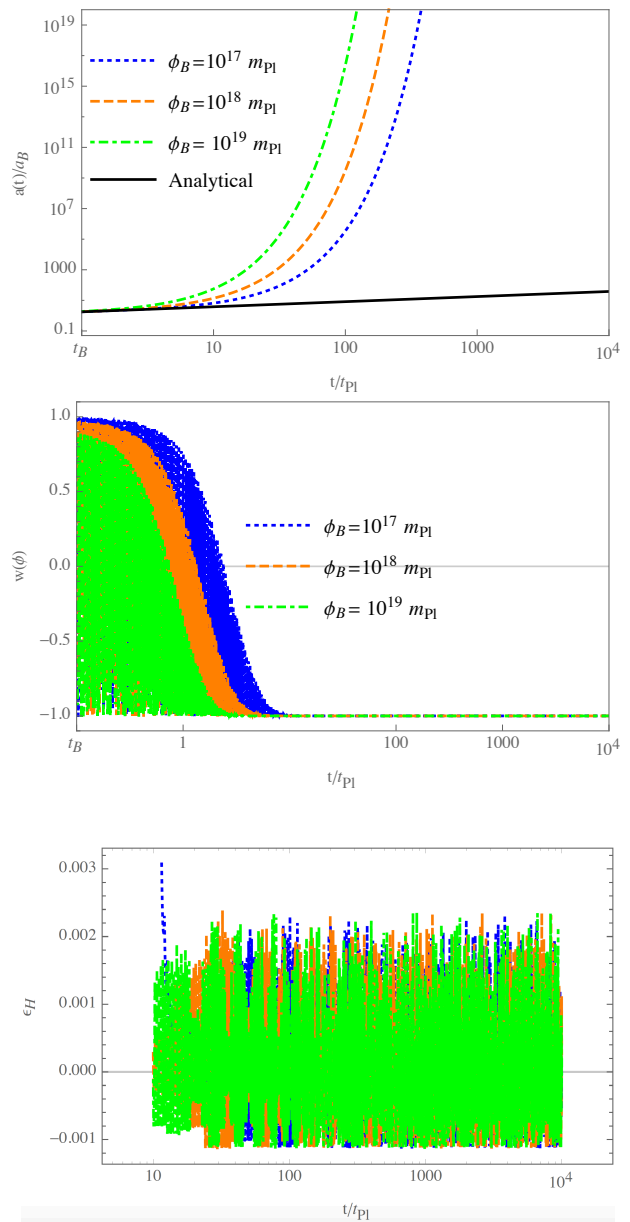


FIG. 9. Numerical solution for the potential energy dominated initial conditions for the power law potential with $n = 1/2$ and $\dot{\phi}_B > 0$. Top panel: the evolution of the scale factor $a(t)$ including the analytical solution given by Eq. (3.4). Middle panel: the equation of state $w(\phi)$. Bottom panel: the slow-roll parameter ϵ_H .

ϕ_B but with different signs of $\dot{\phi}_B$. Again, similar to the last two cases, the evolutions of the background can be divided into three different phases, the bouncing, transition and slow-roll inflation, as one can see clearly from the behavior of the equation of state $w(\phi)$. Moreover, during the bouncing phase the evolution of the scale factor $a(t)$ is universal: *it does not depend on the initial values of ϕ_B and $\dot{\phi}_B$, neither on the form of potentials.* As long

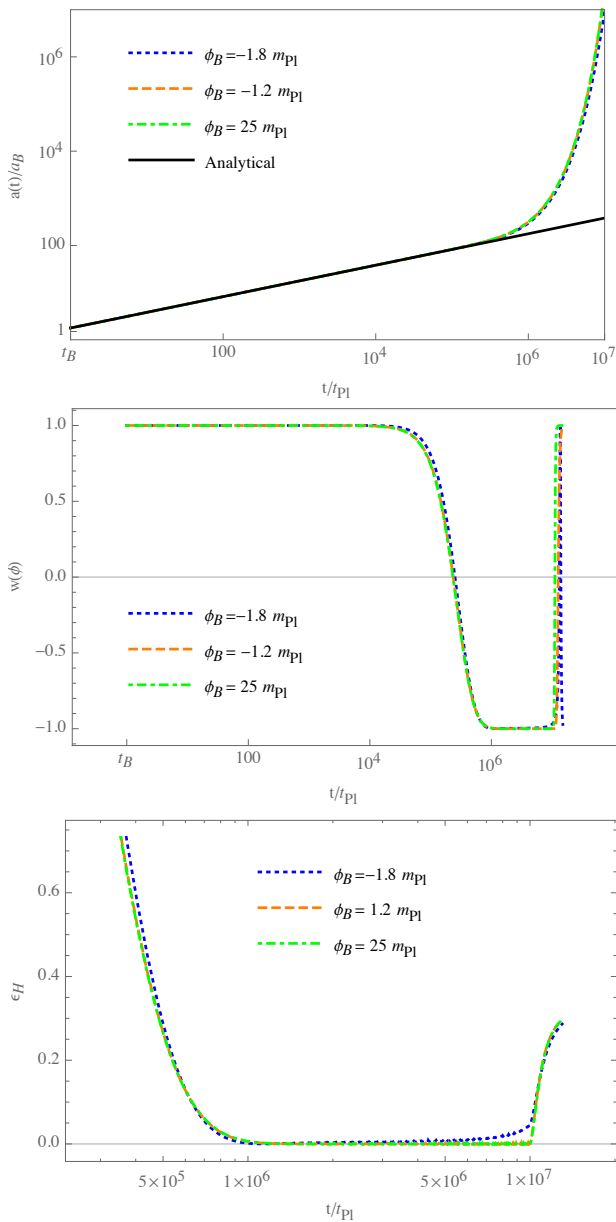


FIG. 10. Numerical solution for the Starobinsky potential with $\dot{\phi}_B > 0$. Top panel: the evolution of the scale factor $a(t)$ and the analytical solutions given by Eq. (3.4). Middle panel: the equation of state $w(\phi)$. Bottom panel: the slow-roll parameter ϵ_H .

as the evolution is dominated by the kinetic energy of the inflaton, the evolution of $a(t)$ is well described by the analytical solution (3.4) during the bouncing phase, no matter whether the inflationary potential is the Starobinsky one or the power-law one!

From Fig. 12 it can be seen that the universality is closely related to the fact that the kinetic energy of the inflaton dominates the evolution of the background during the whole bouncing phase, once it dominates at the quantum bounce. Then, the kinetic energy suddenly decreases at $t/t_{Pl} \simeq 10^5$, and the potential energy starts to

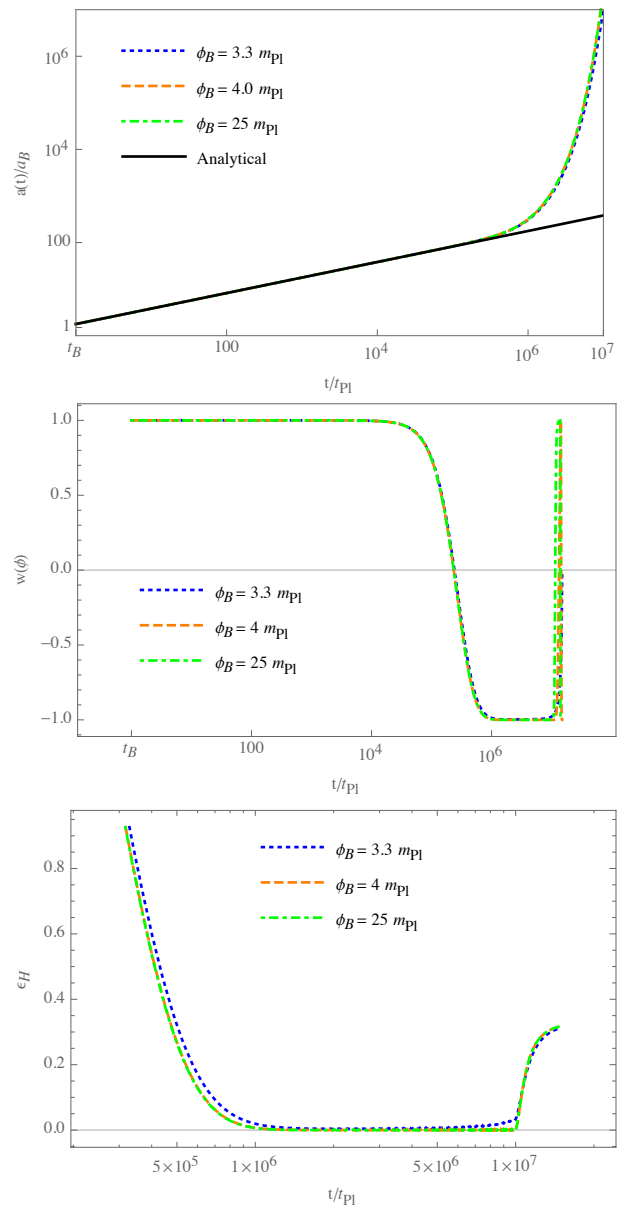


FIG. 11. Numerical solution for the theory of Starobinsky potential with $\dot{\phi}_B < 0$. Top panel: the evolution of the scale factor $a(t)$ from both the numerical and analytical solutions. Middle panel: the equation of state $w(\phi)$ for the same set of initial conditions. Bottom panel: the slow-roll parameter ϵ_H during the slow-roll inflation.

take over ($w(\phi) \simeq -1$), whereafter the slow-roll inflation starts, as one can see clearly from Figs. 10 and 11.

The initial conditions that lead to sufficiently long slow-roll inflation are shown in Fig. 13, from which we can see that, in order to produce at least 60 e-folds during the slow-roll inflation, the values of ϕ_B have to be in the range of

$$\phi_B \in (-1.47m_{Pl}, +\infty) \quad (2.18)$$

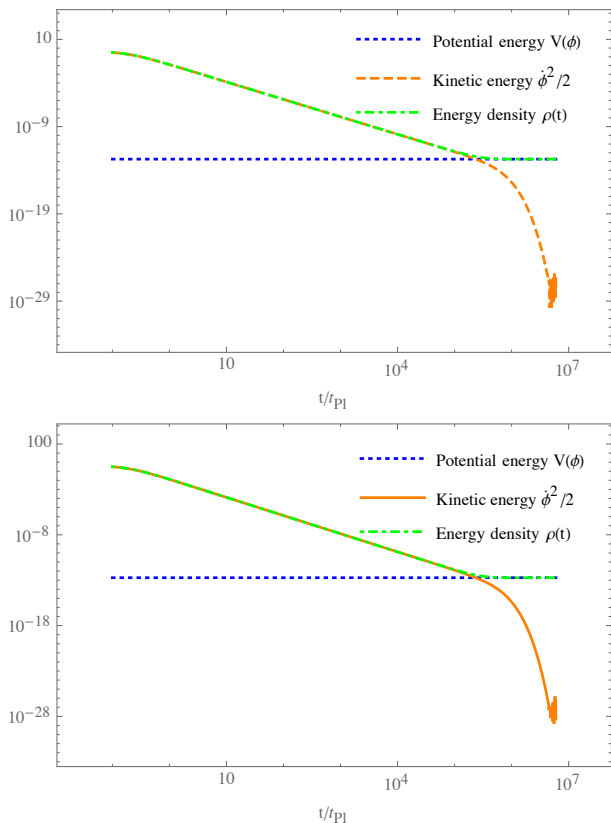


FIG. 12. Comparison between the potential energy $V(\phi)$ and the kinetic energy $\dot{\phi}^2/2$ for the theory of Starobinsky potential. Top panel: for the initial condition $\phi_B = 4m_{\text{Pl}}$ and $\dot{\phi}_B > 0$. Bottom panel: for the initial condition $\phi_B = 9m_{\text{Pl}}$ and $\dot{\phi}_B < 0$.

for $\dot{\phi}_B > 0$, and

$$\phi_B \in (3.61m_{\text{Pl}}, +\infty) \quad (2.19)$$

for $\dot{\phi}_B < 0$. Within the above ranges, Fig. 13 shows that the e-folds N_{inf} increases when the value of ϕ_B increases.

However, in contrast to the power-law potential cases, now the potential energy dominated initial conditions cannot lead to a slow-roll inflation, as can be seen clearly from Fig. 14. This is consistent with what was obtained in [30, 31].

D. Summary of the background evolution of the FLRW universe

Before proceeding further, let us summarize the main results obtained so far on the background evolutions of the flat FLRW universe in the framework of the dressed metric approach in LQC. The evolutions can be divided into two classes, one is dominated by the kinetic energy of the inflaton at the quantum bounce, and the other is dominated by its potential energy at the bounce.

In the case where the evolution of the universe is dominated by the potential energy of the inflaton, a slow-roll

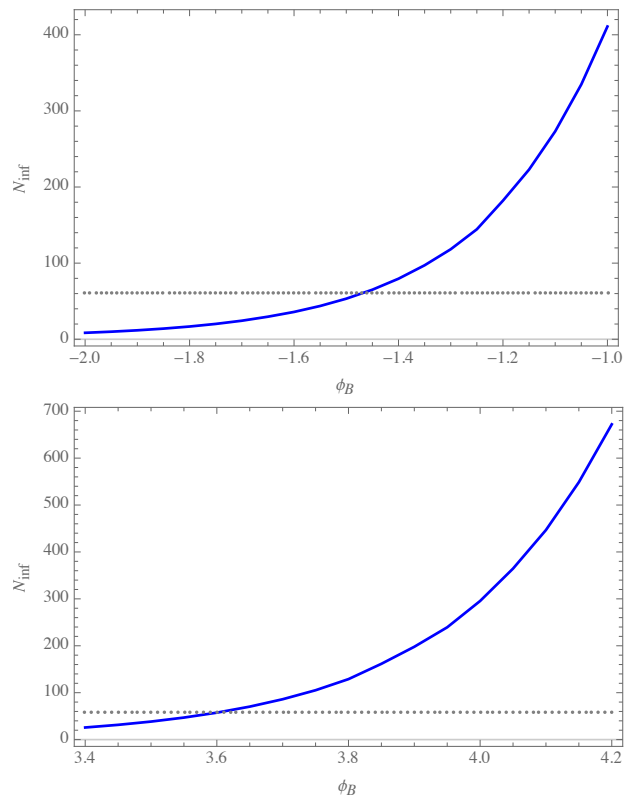


FIG. 13. The e-folds N_{inf} during the slow-roll inflation as a function of ϕ_B . Top panel: for $\phi_B > 0$. Bottom panel: for $\phi_B < 0$.

inflation phase may or may not be possible, depending on the inflationary models. In particular, for the power-law potential, it is always the case, but for the Starobinsky potential the evolution never leads to a slow-roll inflationary phase [30, 31].

In contrast, a slow-roll inflationary phase is always achieved in the case where the evolution of the universe is dominated initially by the kinetic energy of the inflaton at the quantum bounce. In this case, the evolution of the universe prior to preheating always experiences three different phases, *the bouncing, transition and slow-roll inflation*, as it can be seen clearly from the equation of state $w(\phi)$ shown in Figs. 1, 5, 6, 10 and 11. To see this more clearly, we collect these results together in Fig. 15. Note that, instead of plotting the case of the power-law potential with $n = 1/2$, we plotted out the case with $n = 1/3$ in order to show further the universal properties of the evolution.

It is also remarkable to note that during the bouncing phase the evolution of the scale factor $a(t)$ with the kinetic energy dominated initial conditions is universal: it is not only independent of the initial conditions ϕ_B and $\dot{\phi}_B$, but also independent of the inflationary potentials, as shown explicitly in Figs. 1, 5, 6, 10 and 11. For the sake of comparison, we collect these curves into a single figure, Fig. 16. The main reason is that the po-

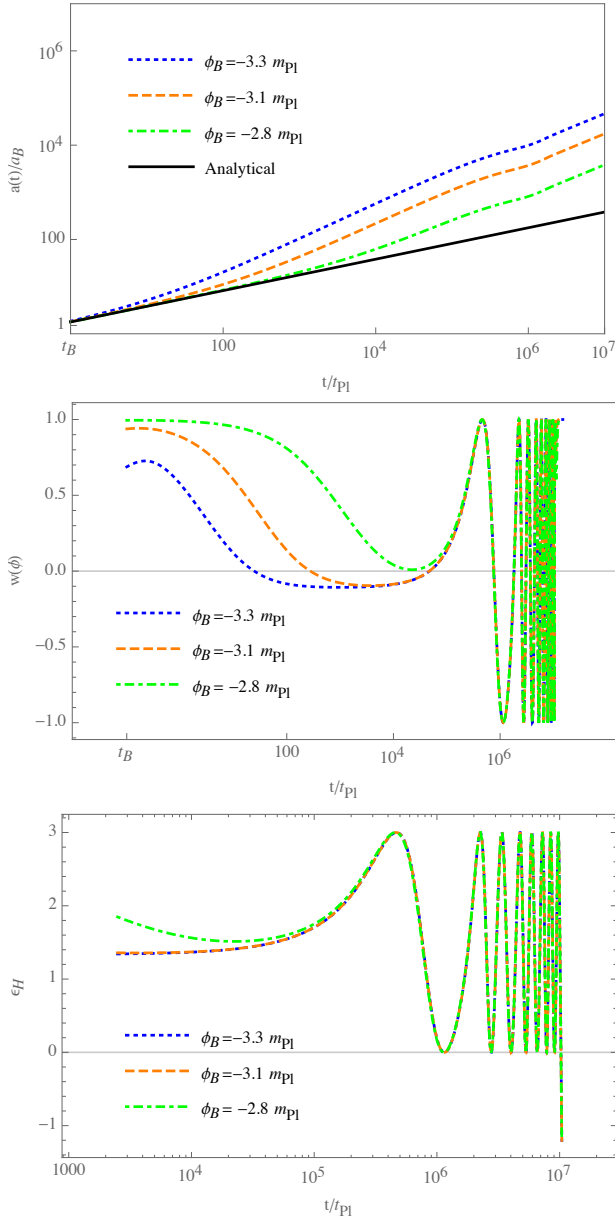


FIG. 14. Numerical solution for the Starobinsky potential with the potential energy dominated initial conditions. For the sake of simplicity, we show here only for $\dot{\phi}_B > 0$. Top panel: the evolution of the scale factor $a(t)$ and the analytical solution of Eq. (3.4). Middle panel: the equation of state $w(\phi)$. Bottom panel: the slow-roll parameter ϵ_H .

tential energy $V(\phi)$ remains very small and the kinetic energy is completely dominant during this whole phase. For example, for the potential $V(\phi) = V_0\phi^2$, we find that $V(\phi)/m_{\text{Pl}}^4 \in (2 \times 10^{-11}, 4.5 \times 10^{-11})$; for $n = 1/3$, $V(\phi)/m_{\text{Pl}}^4 \in (9 \times 10^{-12}, 1.2 \times 10^{-11})$; and for the Starobinsky potential, we have $V(\phi)/m_{\text{Pl}}^4 \in (7 \times 10^{-13}, 7.3 \times 10^{-13})$. Clearly, in this whole phase, we can safely ignore the effects of the potential and simply set it to zero, $V(\phi) = 0$. This explains why the evolution of $a(t)$ is independent of inflationary models during this bouncing

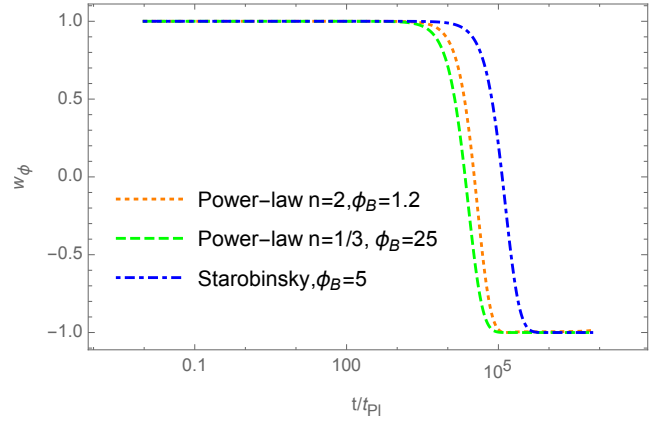


FIG. 15. The equation of state w_ϕ for the power-law and Starobinsky potentials. We choose $m = 1.3 \times 10^{-6}$ for $n = 2$, $m = 1.1 \times 10^{-3}$ for $n = 1/3$, and $M = 2.5 \times 10^{-6}$ for the Starobinsky potential. In all the cases we set $m_{\text{Pl}} = 1$.

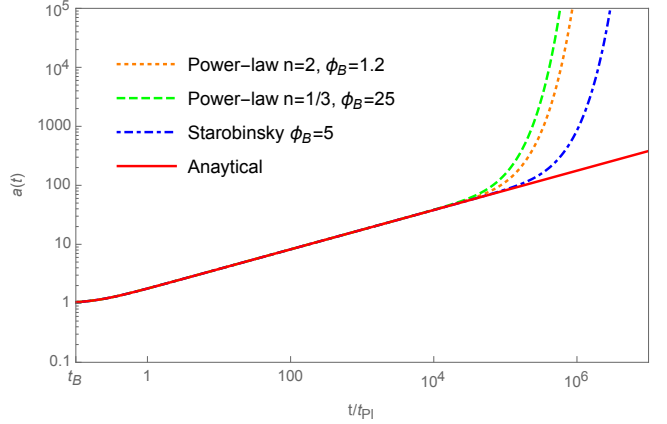


FIG. 16. The evolution of the scale factor $a(t)$ in the case where the evolution is dominated by the kinetic energy of the inflaton at the quantum bounce for the power-law and Starobinsky potentials. The parameters are chosen as the same as those given in Fig. 15.

phase.

During the bouncing phase, the universe expands about 4 e-folds, and the exact number depends on the choices of initial conditions of ϕ_B and $\dot{\phi}_B$, as well as on the inflationary models (for details, see the analysis to be carried out in the next section). Afterwards, the kinetic energy drops dramatically (about 12 orders from its initial Planck scale), so the equation of state $w(\phi)$ suddenly changes from $w(\phi) \simeq +1$ to $w(\phi) \simeq -1$, whereby the slow-roll inflationary phase starts. The transition phase is normally very short in comparison to the other two phases.

III. BACKGROUND EVOLUTION: ANALYTICAL

As shown numerically in the last section, a slow-roll inflationary phase can be achieved for any potential considered so far only for the case where the kinetic energy of the inflaton dominates the evolution of the universe at the quantum bounce. Therefore, in the rest of this paper we shall mainly focus on this case. Then, the evolution of the background can be divided into three phases, the bouncing, transition, and slow-roll inflation. In the following we shall first find analytical solutions of the scale factor in each of these three phases, and then connect them smoothly across the boundaries of these phases.

A. The Bouncing Phase

Since the kinetic energy of the inflaton is dominating during this phase, as shown in the last section, we can safely ignore the effects of the potential term in the equations of motion, and find

$$H^2 = \frac{8\pi}{3m_{\text{Pl}}^2} \frac{1}{2} \dot{\phi}^2 \left(1 - \frac{\dot{\phi}^2}{2\rho_c} \right), \quad (3.1)$$

$$\ddot{\phi} + 3H\dot{\phi} = 0. \quad (3.2)$$

The above set of equations can be solved analytically. In particular, from the Klein-Gordon equation (3.2) we obtain

$$\dot{\phi}(t) = \pm \sqrt{2\rho_c} \left(\frac{a_B}{a(t)} \right)^3. \quad (3.3)$$

Substituting this into Eq. (3.1), we find

$$a(t) = a_B \left(1 + \gamma_B \frac{t^2}{t_{\text{Pl}}^2} \right)^{1/6}, \quad (3.4)$$

where $\gamma_B \equiv \frac{24\pi\rho_c}{m_{\text{Pl}}^4} \simeq 30.9$ is a dimensionless constant. The relation between the conformal time η and the cosmic time t is then given by

$$\eta(t) - \eta_B = {}_2F_1 \left(\frac{1}{6}, \frac{1}{2}, \frac{3}{2}; -\gamma_B \frac{t^2}{t_{\text{Pl}}^2} \right) t, \quad (3.5)$$

which is a monotonically increasing function of t , where ${}_2F_1(a, b, c; z)$ is the hypergeometric function. With the analytical solution for $a(t)$, from Eq. (3.3) one finds

$$\phi(t) = \phi_B \pm \frac{m_{\text{Pl}}}{2\sqrt{3}\pi} \text{arcsinh} \left(\sqrt{\gamma_B} \frac{t}{t_{\text{Pl}}} \right), \quad (3.6)$$

and

$$\dot{\phi}(t) = \pm \frac{\sqrt{2\rho_c}}{(1 + \gamma_B t^2/t_{\text{Pl}}^2)^{1/2}}. \quad (3.7)$$

In the top panels of Figs. 1, 5, 6, 10, and 11, we compared the analytical solution of the scale factor given by

Eq. (3.4) with the numerical (exact) one, obtained by various initial conditions and potentials, and found that all the numerical solutions are universal, and can be described well by the analytical solution.

Note that, in contrast to the kinetic energy dominated bouncing phase, for the potential dominated bouncing, as shown in Figs. 4, 9 and 14, the universality of the evolution of $a(t)$ is lost, and it sensitively depends on the initial conditions specified by ϕ_B and $\dot{\phi}_B$, as well as the inflationary potential $V(\phi)$.

B. The Transition Phase

After the bouncing phase, the universe enters the transition phase. During this period, the kinetic energy of the scalar field decreases dramatically, and the potential energy soon becomes dominant. A special point during this process is the time t_c , when the potential energy is equal to the kinetic energy, i.e., $w(\phi(t_c)) = 0$. As shown by the numerical results, the variations of both the e -folds δN and the scalar field ϕ during the transition phase are almost negligible, in comparison to those obtained during the bouncing and slow-roll inflationary phases. This implies that the analytical solutions of the scale factor $a(t)$ and scalar field $\phi(t)$ given by, respectively, Eqs. (3.4) and (3.6) for the bouncing phase can extend their validity until $t = t_c$. In particular, we have

$$\dot{\phi}_c \simeq \pm \frac{\sqrt{2\rho_c}}{(1 + \gamma_B t_c^2/t_{\text{Pl}}^2)^{1/2}}, \quad (3.8)$$

where $\phi_c \equiv \phi(t_c)$. On the other hand, since $w(\phi(t_c)) = 0$, we have

$$\dot{\phi}_c = \pm \sqrt{2V(\phi_c)}. \quad (3.9)$$

Then, combining the above two equations we can find ϕ_c in terms of t_c . To show this, let us first note the examples in the second figures of Figs. 1, 5, 6, 10 and 11, from which we find that $t_c/t_{\text{Pl}} \simeq 10^4 - 10^5$ (locating at points when $w_\phi \sim 0$ at these figures), that is, in general we have $t_{\text{Pl}}/t_c \ll 1$. Then, to the leading order of t_{Pl}/t_c , we find that,

$$\begin{aligned} \phi_c &= \phi_B \pm \frac{m_{\text{Pl}}}{2\sqrt{3}\pi} \text{arcsinh} \left(\sqrt{\gamma_B} \frac{t_c}{t_{\text{Pl}}} \right) \\ &\simeq \phi_B \pm \frac{m_{\text{Pl}}}{2\sqrt{3}\pi} \ln \left(2\sqrt{\gamma_B} \frac{t_c}{t_{\text{Pl}}} \right), \end{aligned} \quad (3.10)$$

$$\begin{aligned} \dot{\phi}_c &= \pm \sqrt{\frac{\gamma_B m_{\text{Pl}}^4}{12\pi(1 + \gamma_B t_c^2/t_{\text{Pl}}^2)}} \\ &\simeq \pm \frac{m_{\text{Pl}}^2}{\sqrt{12\pi}} \frac{t_{\text{Pl}}}{t_c}. \end{aligned} \quad (3.11)$$

With these expressions, t_c can be found explicitly for the quadratic and Starobinsky potentials. In particular, for

the quadratic potential from Eq. (3.9) we obtain

$$t_c = \begin{cases} \frac{1}{mW(2\sqrt{\gamma_B} \frac{m_{\text{Pl}}}{m} e^{2\sqrt{3\pi}\phi_B/m_{\text{Pl}}})}, & \dot{\phi}_c > 0, \\ \frac{-1}{mW_{-1}(-2\sqrt{\gamma_B} \frac{m_{\text{Pl}}}{m} e^{-2\sqrt{3\pi}\phi_B/m_{\text{Pl}}})}, & \dot{\phi}_c < 0, \end{cases} \quad (3.12)$$

$$t_c = \begin{cases} \frac{2}{3M} + \frac{e^{-\frac{2\sqrt{3\pi}\phi_B}{m_{\text{Pl}}}} \left[\left(\sqrt{36\gamma_B m_{\text{Pl}}^2 e^{\frac{4\sqrt{3\pi}\phi_B}{m_{\text{Pl}}}} - 3M^2 + 6\sqrt{\gamma_B} m_{\text{Pl}} e^{\frac{2\sqrt{3\pi}\phi_B}{m_{\text{Pl}}}} \right)^{2/3} + (3M^2)^{1/3} \right]}{2(9M)^{1/3} \sqrt{\gamma_B} m_{\text{Pl}} \left(\sqrt{36\gamma_B m_{\text{Pl}}^2 e^{\frac{4\sqrt{3\pi}\phi_B}{m_{\text{Pl}}}} - 3M^2 + 6\sqrt{\gamma_B} m_{\text{Pl}} e^{\frac{2\sqrt{3\pi}\phi_B}{m_{\text{Pl}}}} \right)^{1/3}}, & \dot{\phi}_c > 0, \\ \frac{2}{3M} \left[1 + \left(\frac{4\sqrt{\gamma_B} m_{\text{Pl}}}{3M} \right)^{2/3} e^{-\sqrt{16\pi/3}\phi_B/m_{\text{Pl}}} \right], & \dot{\phi}_c < 0. \end{cases} \quad (3.13)$$

The detailed derivation of t_c for the Starobinsky potential is presented in Appendix A.

Given t_c , we are now able to calculate $a(t_c)$, $\phi(t_c)$ and $\dot{\phi}(t_c)$, which are given by

$$a_c = a_B \left(1 + \gamma_B \frac{t_c^2}{t_{\text{Pl}}^2} \right)^{1/6}, \quad (3.14)$$

$$\phi_c = \phi_B + \frac{m_{\text{Pl}}}{2\sqrt{3\pi}} \ln \left(2\sqrt{\gamma_B} \frac{t_c}{t_{\text{Pl}}} \right), \quad (3.15)$$

and

$$\dot{\phi}_c = \frac{mm_{\text{Pl}}}{2\sqrt{3\pi}} W \left(2\sqrt{\gamma_B} \frac{m_{\text{Pl}}}{m} e^{2\sqrt{3\pi}\phi_B/m_{\text{Pl}}} \right). \quad (3.16)$$

Then, we obtain,

$$N_c \equiv \ln \left(\frac{a_c}{a_B} \right) = \frac{1}{6} \ln \left[1 + \frac{\gamma_B m_{\text{Pl}}^2}{m^2 W \left(2\sqrt{\gamma_B} \frac{m_{\text{Pl}}}{m} e^{2\sqrt{3\pi}\phi_B/m_{\text{Pl}}} \right)^2} \right]. \quad (3.17)$$

The numerical values of N_c , ϕ_c , and $\dot{\phi}_c$ derived from the above expressions are presented in Table. I-IV for different potentials and signs of $\dot{\phi}_c$. From these tables it can be seen that the upper bounds of errors of these quantities between their numerical (exact) and analytical values are less than one percent.

Right after the moment $t = t_c$, the kinetic energy of the scalar field is continuously decreasing, and the universe remains decelerating until $w = -1/3$, at which point we have

$$\ddot{a}(t) = 0, \quad \dot{\phi}^2 = V(\phi), \quad (w(\phi) = -1/3). \quad (3.18)$$

Denoting this moment as t_i , we can see that after this moment the universe enters an accelerating phase, $\ddot{a}(t) > 0$. Right after t_i , the slow-roll parameter $|\epsilon_H|$ is still large and oscillating around its zero point, but soon becomes very small, $|\epsilon_H| \ll 1$, and then the slow-roll inflationary

phase starts. Therefore, practically we can consider the moment $t = t_i$ as the beginning of the slow-roll inflation. To estimate the values of $\phi(t_i)$ and $a(t_i)$, we expand $\phi(t)$ and $a(t)$ at $t = t_c$ as

$$\phi(t) = \phi_c + t_c \dot{\phi}_c \ln \frac{t}{t_c}, \quad (3.19)$$

$$a(t) = a_c \left(1 + t_c H_c \ln \frac{t}{t_c} \right), \quad (3.20)$$

where H_c can be calculated by using the Friedmann equation,

$$H_c = \sqrt{\frac{8\pi G}{3} \left(\frac{\dot{\phi}_c^2}{2} + V(\phi_c) \right)}. \quad (3.21)$$

Note that in writing the above equation we had ignored the term $\rho(t_c)/\rho_c$ in Eq. (2.2), which is of the order $\rho(t_c)/\rho_c \simeq 10^{-12}$, as shown in the last section. Then, at $t = t_i$ we have

$$\phi_i = \phi_c + \dot{\phi}_c t_c \ln \frac{t_i}{t_c}, \quad (3.22)$$

$$\dot{\phi}_i = \frac{t_c}{t_i} \dot{\phi}_c. \quad (3.23)$$

Given $w = -1/3$ at $t = t_i$, we also have

$$\dot{\phi}_i^2 = V(\phi_i). \quad (3.24)$$

In general it is very difficult to solve above equations to get t_i for any given potential $V(\phi)$. However, we can always expand $V(\phi_i)$ at ϕ_c as

$$V(\phi_i) = V(\phi_c) + V_{,\phi}(\phi_c) t_c \dot{\phi}_c \ln \frac{t_i}{t_c}, \quad (3.25)$$

and Eq. (3.24) yields

$$\dot{\phi}_c = \pm \frac{t_i}{t_c} \left(\sqrt{V(\phi_c)} + \frac{t_c \dot{\phi}_c}{2} \frac{V_{,\phi}(\phi_c)}{\sqrt{V(\phi_c)}} \ln \frac{t_i}{t_c} \right), \quad (3.26)$$

where “ \pm ” correspond to $\dot{\phi}_c > 0$ and $\dot{\phi}_c < 0$, respectively. Solving the above equations we find

TABLE I. Numerical and analytical results with different values of ϕ_B for a quadratic potential and $\dot{\phi}_B > 0$. We use units $m_{\text{Pl}} = 1$ and $a_B = 1$.

ϕ_B	1.2	3	6	8	10	15	30	100
ϕ_c (num.)	3.27857	5.01001	7.93546	9.89956	11.8701	16.8135	31.7103	101.52
ϕ_c in Eq. (3.15)	3.30919	5.04065	7.96612	9.93022	11.9007	16.8442	31.741	101.552
relative errors (%)	0.933958	0.611686	0.386329	0.309709	0.258305	0.182371	0.0966972	0.00315
$10^6 \dot{\phi}_c$ (num.)	4.26214	6.513	10.3161	12.8694	15.4311	21.8575	41.2234	131.98
$10^6 \dot{\phi}_c$ in Eq. (3.16)	4.30195	6.55285	10.356	12.9093	15.471	21.8974	41.2633	132.017
relative errors (%)	0.933974	0.611895	0.386329	0.309711	0.258344	0.18245	0.0967077	0.02803
N_c (num.)	4.08222	3.9431	3.79139	3.71822	3.65808	3.54258	3.33171	2.94444
N_c in Eq. (3.17)	4.08574	3.94546	3.79291	3.71945	3.65911	3.54331	3.3321	2.94445
relative error (%)	0.0862255	0.0598019	0.0399598	0.0328818	0.0280036	0.0205946	0.0117816	0.00034
ϕ_i (num.)	3.31229	5.04457	7.97064	9.93496	11.9056	16.8493	31.7463	101.557
ϕ_i in Eq. (3.29)	3.41687	5.15005	8.07676	10.0413	12.0121	16.956	31.8533	101.664
relative errors (%)	3.15746	2.09092	1.33138	1.07037	0.89445	0.633335	0.336934	0.105518
N_i (num.)	4.18948	4.05307	3.90334	3.83086	3.77119	3.65638	3.44632	3.05956
N_i in Eq. (3.30)	4.2849	4.1475	3.99703	3.9243	3.86445	3.74938	3.53901	3.15202
relative error (%)	2.27761	2.32974	2.40028	2.43898	2.47292	2.54341	2.6897	3.02191

TABLE II. Numerical and analytical results with different values of ϕ_B for a quadratic potential and $\dot{\phi}_B < 0$. We use units $m_{\text{Pl}} = 1$ and $a_B = 1$.

ϕ_B	5.3	6	8	10	12	15	30	40
ϕ_c (num.)	3.21517	3.94896	6.01803	8.06595	10.1027	13.1457	28.2707	38.3202
ϕ_c in Eq. (3.15)	3.18455	3.91832	5.98738	8.03529	10.0721	13.1151	28.24	38.2896
relative errors (%)	0.952133	0.775671	0.509318	0.380079	0.303482	0.233247	0.108462	0.080017
$10^6 \dot{\phi}_c$ (num.)	-4.17972	-5.13364	-7.82344	-10.4857	-13.1336	-17.0895	-36.7519	-49.8163
$10^6 \dot{\phi}_c$ in Eq. (3.16)	-4.13992	-5.09382	-7.78359	-10.4459	-13.0937	-17.0496	-36.712	-49.7765
relative errors (%)	0.961286	0.781726	0.511909	0.381523	0.304391	0.233919	0.108579	0.0800772
N_c (num.)	4.1026	4.03269	3.89019	3.79158	3.71595	3.62766	3.37149	3.2699
N_c in Eq. (3.16)	4.09854	4.02942	3.88809	3.79003	3.71472	3.62672	3.37106	3.26958
relative errors (%)	0.0992386	0.0811183	0.0540453	0.0409425	0.0331148	0.0258796	0.0127129	0.00960974
ϕ_i (num.)	3.17574	3.91015	5.98013	8.02847	10.0655	13.1087	28.234	38.2837
ϕ_i in Eq. (3.29)	3.12504	3.85941	5.92935	7.97768	10.0147	13.0579	28.1832	38.2329
relative errors (%)	1.59655	1.29764	0.849147	0.632656	0.504679	0.387547	0.179945	0.132708
N_i (num.)	4.22812	4.1562	4.01083	3.91087	3.83446	3.74546	3.48806	3.38619
N_i in Eq. (3.30)	4.21348	4.14326	4.00032	3.9015	3.82575	3.73735	3.48099	3.37935
relative error (%)	0.346113	0.311432	0.261958	0.239621	0.227182	0.216663	0.202858	0.202082

$$t_i = \begin{cases} \frac{2\sqrt{V(\phi_c)}}{V_\phi(\phi_c)W\left[\frac{2\sqrt{V(\phi_c)}}{V_\phi(\phi_c)t_c}\exp\left(\frac{2V(\phi_c)}{t_c\phi_c V_\phi(\phi_c)}\right)\right]}, & \dot{\phi}_c > 0, \\ -\frac{2\sqrt{V(\phi_c)}}{V_\phi(\phi_c)W_{-1}\left[-\frac{2\sqrt{V(\phi_c)}}{V_\phi(\phi_c)t_c}\exp\left(\frac{2V(\phi_c)}{t_c\phi_c V_\phi(\phi_c)}\right)\right]}, & \dot{\phi}_c < 0. \end{cases} \quad (3.27)$$

Once t_i is given, we can then calculate a_i and ϕ_i , which are given by

$$a_i = a_c \left(1 + t_c H_c \ln \frac{t_i}{t_c}\right), \quad (3.28)$$

$$\phi_i = \phi_c + t_c \dot{\phi}_c \ln \frac{t_i}{t_c}. \quad (3.29)$$

Then, we find that

$$\begin{aligned} N_i &\equiv \ln \left(\frac{a_i}{a_B}\right) \\ &= N_c + \ln \left(1 + t_c H_c \ln \frac{t_i}{t_c}\right). \end{aligned} \quad (3.30)$$

The numerical values of ϕ_i and N_i obtained from the above expressions and the numerical ones are presented

TABLE III. Numerical and analytical results with different values of ϕ_B for the Starobinsky potential and $\dot{\phi}_B > 0$. We use units $m_{\text{Pl}} = 1$ and $a_B = 1$.

ϕ_B	-1.47	-1.30	-1.1	-0.4	0.1	0.2	1	4
ϕ_c (num.)	0.928828	1.09732	1.29648	1.99585	2.49582	2.59582	3.39582	6.39582
ϕ_c in Eq. (3.15)	0.959718	1.1281	1.3272	2.02652	2.52649	2.62649	3.42648	6.42648
relative errors (%)	3.32573	2.80515	2.36924	1.53662	1.22872	1.18138	0.903066	0.47948
$10^6 \phi_c$ (num.)	0.599505	0.606327	0.610156	0.613022	0.613174	0.613181	0.613196	0.613196
$10^6 \phi_c$ in Eq. (3.16)	0.601132	0.60714	0.610515	0.613043	0.613176	0.613183	0.613196	0.613196
relative errors (%)	0.271265	0.134118	0.0588624	0.00335137	0.000448314	0.000301966	0.0000209013	$4.22436 * 10^{-6}$
N_c (num.)	4.73968	4.73738	4.73611	4.73516	4.73511	4.73511	4.73511	4.7351
N_c in Eq. (3.16)	4.74174	4.73843	4.73658	4.7352	4.73513	4.73513	4.73512	4.73512
relative errors (%)	0.0434831	0.0220978	0.00990369	0.000787333	0.000327793	0.000309995	0.000270085	0.000286131
ϕ_i (num.)	0.964351	1.13323	1.33261	2.03215	2.53212	2.63212	3.43212	6.43212
ϕ_i in Eq. (3.29)	1.01542	1.18417	1.38348	2.08296	2.58293	2.68293	3.48293	6.48293
relative errors (%)	5.29573	4.4954	3.8172	2.50043	2.00661	1.93038	1.48042	0.789942
N_i (num.)	4.85272	4.85166	4.85108	4.85066	4.85063	4.85063	4.85063	4.85063
N_i in Eq. (3.30)	4.8497	4.84707	4.8456	4.84451	4.84445	4.84445	4.84444	4.84444
relative error (%)	0.0622625	0.094637	0.113005	0.126749	0.127458	0.127488	0.127546	0.127531

TABLE IV. Numerical and analytical results with different values of ϕ_B for the Starobinsky potential and $\dot{\phi}_B < 0$. We use units $m_{\text{Pl}} = 1$ and $a_B = 1$.

ϕ_B	3.61	3.7	3.8	3.9	4.1	4.3	5	8
ϕ_c (num.)	1.21293	1.30332	1.40361	1.50381	1.70402	1.90411	2.60418	5.60418
ϕ_c in Eq. (3.15)	1.18224	1.27263	1.37293	1.47313	1.67335	1.87344	2.57351	5.57352
relative errors (%)	2.53051	2.35464	2.18599	2.04003	1.79998	1.61067	1.1776	0.547214
$10^6 \phi_c$ (num.)	-0.608918	-0.61024	-0.611236	-0.611895	-0.612623	-0.612943	-0.613182	-0.613195
$10^6 \phi_c$ in Eq. (3.16)	-0.608407	-0.609875	-0.610986	-0.611727	-0.612547	-0.61291	-0.61318	-0.613196
relative errors (%)	0.0838578	0.0599164	0.0407656	0.0274843	0.0123245	0.00546677	0.000304264	0.000112727
N_c (num.)	4.73794	4.73706	4.7364	4.73596	4.73548	4.73527	4.73511	4.7351
N_c in Eq. (3.16)	4.73773	4.73693	4.73632	4.73592	4.73547	4.73527	4.73513	4.73512
relative errors (%)	0.00437058	0.0027701	0.00166291	0.000973656	0.000256096	0.0000465156	0.00026842	0.000294261
ϕ_i (num.)	1.17634	1.26682	1.36718	1.46742	1.66768	1.86779	2.56788	5.56788
ϕ_i in Eq. (3.29)	1.12548	1.21597	1.31634	1.41659	1.61686	1.81698	2.51707	5.51707
relative errors (%)	4.32418	4.01394	3.71831	3.46372	3.0472	2.72049	1.97868	0.912557
N_i (num.)	4.85439	4.85322	4.85234	4.85177	4.85113	4.85085	4.85064	4.85063
N_i in Eq. (3.30)	4.84764	4.84665	4.8459	4.84541	4.84487	4.84463	4.84445	4.84444
relative error (%)	0.138954	0.135372	0.13271	0.130961	0.129044	0.128204	0.127572	0.12753

in Table. I-IV for different potentials (quadratic and Starobinsky potentials) and signs of $\dot{\phi}_c$, from which it can be seen that the upper bounds of errors of our analytical estimations for ϕ_i are less than 5.3%, while for N_i they are less than 3.1%.

C. The Slow-Roll Inflationary Phase

After $t = t_i$, the universe soon enters the slow-roll inflationary phase. During it, the potential energy of the scalar field is dominating. To ensure the slow-roll evolution of the background, we also need to impose two additional conditions,

$$(i) \frac{1}{2} \dot{\phi}^2 \ll V(\phi), \quad (ii) |\ddot{\phi}| \ll |H\dot{\phi}|. \quad (3.31)$$

Then, the Friedmann and Klein-Gordon equations can be approximated by

$$H^2 \simeq \frac{8\pi}{3m_{\text{Pl}}^2} V(\phi), \quad (3.32)$$

$$3H\dot{\phi} + \frac{dV(\phi)}{d\phi} \simeq 0. \quad (3.33)$$

From the Friedmann equation for a slowly varying $V(\phi)$, we obtain,

$$a(t) \propto e^{H_{\text{inf}} t}, \quad (3.34)$$

where H_{inf} denotes the Hubble parameter during the slow-roll inflation. Thus, the e-folds N_{inf} can be calculated via the relation

$$N_{\text{inf}} \equiv \ln \left(\frac{a_{\text{end}}}{a_i} \right) = \int_{t_i}^{t_{\text{end}}} H(t) dt$$

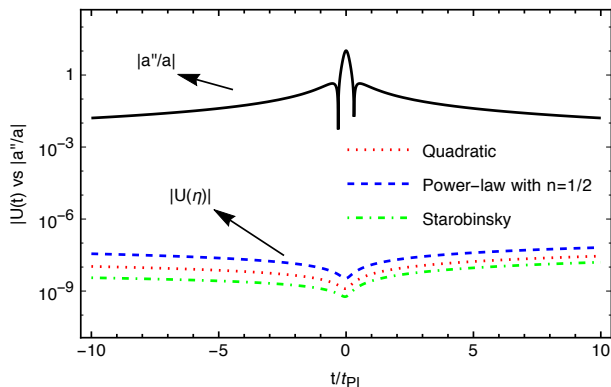


FIG. 17. Comparison between $|U(\eta)|$ and $|a''/a|$ for different inflationary potentials during the bouncing phase for the case where kinetic energy of the inflaton dominates the evolution of the background at the quantum bounce. In plotting these curves, we assumed $\dot{\phi}_B > 0$, and set $\phi_B = 3m_{\text{Pl}}, 5m_{\text{Pl}}, 2m_{\text{Pl}}$, respectively, for the quadratic potential, the power-law potential with $n = 1/2$, and the Starobinsky potential.

$$= \int_{\phi_i}^{\phi_{\text{end}}} \frac{H}{\dot{\phi}} d\phi \simeq \frac{8\pi}{m_{\text{Pl}}^2} \int_{\phi_{\text{end}}}^{\phi_i} \frac{V}{V_{\phi}} d\phi. \quad (3.35)$$

IV. PRIMORDIAL SCALAR AND TENSOR PERTURBATIONS

Let us now turn to consider the linear perturbations of the background of the universe presented in the last two sections. In general, there are mainly two different approaches to implement cosmological perturbations in the framework of LQC, *the dressed metric* [16–18] and *deformed algebra approaches* [13, 49]. In both approaches, the primordial perturbations with quantum gravitational effects have been studied (see, for example, Refs. [18, 30, 31, 44, 45, 53, 55, 56, 61] and references therein). In particular, the deformed algebra approach, with some (reasonable) assumptions, seems already in conflict with current observations [53, 54]. Therefore, in this paper we shall focus ourselves only on *the dressed metric approach*.

A. Cosmological perturbations in the quantum FRLW background spacetime

In this subsection, we present a brief introduction of the dressed metric approach to the cosmological scalar and tensor perturbations in LQC. In the standard inflationary framework, both the cosmological scalar and tensor perturbations are treated as quantum fields in the classical FRLW background spacetime. In this treatment, as the energy density of the background is well below the Planck energy, the quantum gravitational effects of the background spacetime is negligible. However, the above formalism breaks down when one extends the

standard inflationary phase to the pre-inflationary era (near the bounce), in which case the quantum gravitational effects on the background has to be taken into account. For this reason, one has to study the quantum cosmological perturbations on a quantum FRLW background spacetime.

The quantum theory of cosmological perturbations on a quantum FRLW spacetime was developed in the context of LQC in [16–18] based on the framework developed in [15]. In this picture, the quantum cosmological perturbation fields propagate on a quantum geometry described by the quantum state $\Psi_0(a, \phi)$, which is free of singularities. Moreover, as shown in [17], one can treat the cosmological perturbation field as test fields if their back-reaction on the FLRW spacetime is small. In this case, the mathematical treatments can be very much simplified.

In the test field approximation, the dynamics of the cosmological perturbation fields on the quantum geometry $\Psi_0(a, \phi)$ is equivalent to that of quantum fields on a quantum modified effective geometry described by a dressed metric \tilde{g}_{ab} [16–18],

$$\tilde{g}_{ab} dx^a dx^b = \tilde{a}(-d\tilde{\eta}^2 + dx_i dx^i), \quad (4.2)$$

where the dressed scale factor \tilde{a} and the dressed conformal time $\tilde{\eta}$ are

$$\tilde{a} = \left(\frac{\langle \hat{H}_0^{-1/2} \hat{a}^4 \hat{H}_0^{-1/4} \rangle}{\langle \hat{H}_0^{-1} \rangle} \right)^{1/4}, \quad (4.3)$$

$$d\tilde{\eta} = \langle \hat{H}_0^{-1/2} \rangle (\langle \hat{H}_0^{-1/2} \hat{a}^4 \hat{H}_0^{-1/2} \rangle)^{1/2} d\phi. \quad (4.4)$$

Here \hat{H}_0 is the background Hamiltonian and the expectation values are taken with respect to the background quantum geometry state given by $\Psi_0(a, \phi)$. In this dressed metric, the equations of motion of the operators representing scalar and tensor perturbations are formally the same as the equations appearing in classical spacetimes, which in Fourier space are

$$\mu_k^{(s)}(\tilde{\eta})'' + \left(k^2 - \frac{\tilde{a}''}{\tilde{a}} + \tilde{U}(\tilde{\eta}) \right) \mu_k^{(s)}(\tilde{\eta}) = 0, \quad (4.5)$$

and

$$\mu_k^{(t)}(\tilde{\eta})'' + \left(k^2 - \frac{\tilde{a}''}{\tilde{a}} \right) \mu_k^{(t)}(\tilde{\eta}) = 0, \quad (4.6)$$

where $\mu_k^{(s)}(\tilde{\eta}) = z_s \mathcal{R}_k$ with \mathcal{R}_k denotes the cosmological comoving curvature perturbation and $z_s(\tilde{\eta}) = \tilde{a}\dot{\phi}/H$, $\mu_k^{(t)}(\tilde{\eta}) = \tilde{a}h_k$ denotes tensor perturbation, and

$$\tilde{U}(\tilde{\eta}) = \frac{\langle \hat{H}_0^{-1/2} \hat{a}^2 \hat{U}(\phi) \hat{a}^2 \hat{H}_0^{-1/2} \rangle}{\langle \hat{H}_0^{-1/2} \hat{a}^4 \hat{H}_0^{-1/2} \rangle}. \quad (4.7)$$

It should be note that although the effective equation of motions (4.5) and (4.6) takes the same form as their classical version, the background quantities in these equations, namely \tilde{a} , \tilde{U} , and $\tilde{\eta}$ are different from their classical counterparts. In the opposite, these quantities are

now representing the quantum expectation values in the background state $\Psi_0(a, \phi)$. However, it is pointed out in [18] that for sharply peaked background states $\Psi_0(a, \phi)$, the dressed effective quantities (like \tilde{a} , $\tilde{\eta}$, and $\tilde{U}(\tilde{U})$) are very well approximated by their peaked values (a , η , and $U(\phi)$) from the deep Planck era up to the entire expanding phase, where

$$U(\phi) = a^2 (\mathfrak{f}^2 V(\phi) + 2\mathfrak{f}V_{,\phi}(\phi) + V_{,\phi\phi}(\phi)), \quad (4.8)$$

with $\mathfrak{f} \equiv \sqrt{24\pi G \dot{\phi}}/\sqrt{\rho}$. With the above approximation, the equation of motion of the scalar perturbation becomes

$$\mu_k^{(s)}(\eta)'' + \left(k^2 - \frac{a''}{a} + U(\eta)\right) \mu_k^{(s)}(\eta) = 0. \quad (4.9)$$

During the bouncing phase, if the energy density of the scalar field is dominated by its kinetic energy at the quantum bounce, then it will dominate the evolution of the background during the whole bouncing phase, as shown in the last sections. In this case, it can be shown that $U(\eta)$ is negligible in comparison with a''/a . Fig. 17 shows the absolute values of $U(\eta)$ and a''/a for different potentials, from which we can see clearly that $|U(\eta)/(a''/a)| \ll 1$ for any given potentials. Thus, the $U(\eta)$ term in Eq. (4.9) can be safely ignored during the bouncing phase.

In the slow-roll inflationary phase, during which the energy density is dropped down to about $10^{-12}\rho_c$, the equation of motion reduces to the classical one obtained in general relativity,

$$\mu_k^{(s)}(\eta)'' + \left(k^2 - \frac{z_s''}{z_s}\right) \mu_k^{(s)}(\eta) = 0. \quad (4.10)$$

For the tensor perturbations, similar to the scalar one, the equation of motion becomes,

$$\mu_k^{(t)}(\eta)'' + \left(k^2 - \frac{a''}{a}\right) \mu_k^{(t)}(\eta) = 0, \quad (4.11)$$

which takes exactly the same form as that in classical general relativity.

B. The characteristic length during the bouncing phase

The evolutions of the scalar and tensor perturbations depend on both the background and the wave-number k of the perturbations. As we consider only the kinetic energy dominated case, both scalar and tensor perturbations follow the same equation of motion during the bouncing phase ($t/t_{\text{Pl}} \leq 10^4$). In this case, the term a''/a in Eq. (4.9) defines a characteristic radius λ as

$$\lambda^2 = \frac{a}{a''}, \quad (4.12)$$

for $a'' > 0$, which plays the same role as that of the comoving Hubble radius L_H defined as $L_H = (aH)^{-1}$.

However, for a better understanding, we find that, instead of L_H , it is more proper to use λ^2 , as shown schematically in Fig. 18. For example, when the modes are inside this radius (i.e., $1/k^2 < \lambda^2$) the solution of Eq. (4.9) is of the form,

$$\mu_k^{s,t}(\eta) \sim e^{\pm i \int \sqrt{k^2 - a''/a} d\eta}. \quad (4.13)$$

When the modes are outside of the radius (i.e., $1/k^2 > \lambda^2$), we have growing/decaying solutions,

$$\mu_k^{s,t}(\eta) \sim e^{\pm \int \sqrt{a''/a - k^2} d\eta}. \quad (4.14)$$

Here we would like to note that λ^2 is only defined when $a'' > 0$, and right after the bounce a'' changes its sign from positive to negative. This defines two special points $t = \pm t_s$ as shown in Fig. 18, at which we have

$$a''(t_s) = 0. \quad (4.15)$$

Another specific time is the transition point $t = t_i$ which divides the decelerating and accelerating expansions of the universe, i.e., at t_i we have $\ddot{a} = 0$. This point is also considered as the starting point of the slow-roll inflationary phase in this paper.

The term a''/a has its maximum at the bounce, $a''/a|_{t=t_B} = a_B^2 \gamma_B m_{\text{Pl}}^2/3$, which defines a characteristic energy scale,

$$k_B \equiv \sqrt{\frac{a''}{a}} \Big|_{t=t_B} = \sqrt{\frac{\gamma_B}{3}} a_B m_{\text{Pl}}, \quad (4.16)$$

the blue solid curve shown in Fig. 18, so that we can use it to classify different modes. Some modes with large values of $k^2 \gg k_B^2$ (the region below the low (orange) dashed line in Fig. 18) are inside the radius all the time until it exits the Hubble horizon during the slow-roll inflation. Some of the modes with smaller $k^2 \ll k_B^2$ (the region above the upper (green) dashed line in Fig. 18) exit and re-enter the radius during the bouncing phase, and will finally re-exit the Hubble radius during the slow-roll inflation. Since the modes with $k \gg k_B$ are inside the radius during the whole pre-inflationary phase, they will have the same power-law spectra as those given in GR. We are interested in the modes with $k \simeq k_B$ (the shaded region in Fig. 18) as they are modes whose physical energy during the bouncing phase are of the Planck scale $k_{\text{phy}} = k/a_B \simeq m_{\text{Pl}}$. However, the perturbations for these modes have different behavior when they are inside and outside the radius, which makes Eq. (4.9) very difficult to solve analytically.

C. Perturbations During the Bouncing Phase

In general, we can consider the equation of motion of primordial perturbations as a specific type of the Schrödinger equation,

$$\mu_k''(\eta) + [k^2 - \mathcal{V}(\eta)] \mu_k(\eta) = 0, \quad (4.17)$$

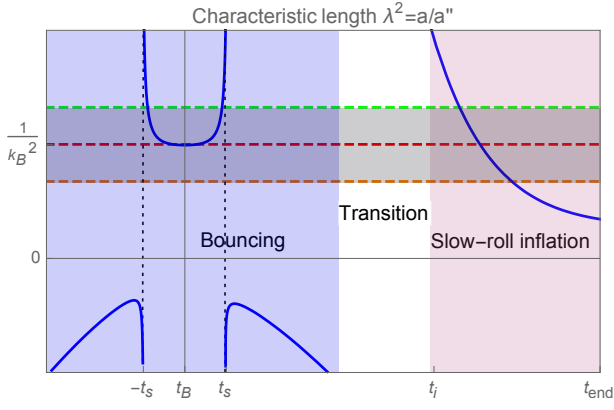


FIG. 18. Schematic plot of a/a'' , where $a''/a|_{t=t_s} = 0$ with $t_s \sim 0.2t_{\text{Pl}}$, $\ddot{a}(t_i) = 0$ with t_i being the starting time of the inflationary phase, and during the slow-roll inflation, $a/a'' = L_{\text{H}}^2/2$. In drawing this figure, we analytically extend the solution of $a(t)$ to a contracting phase $t < t_B$.

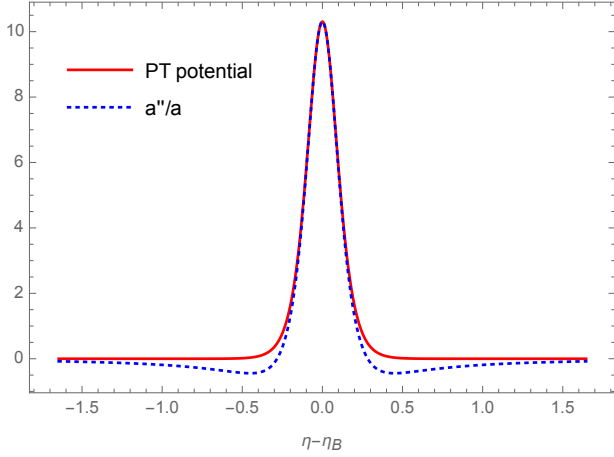


FIG. 19. Comparison between a''/a and the PT potential given in Eq. (4.20). We set $a_B = 1$ and $m_{\text{Pl}} = 1$.

in which $\mathcal{V}(\eta)$ serves as an effective potential, and for the scalar and tensor perturbations we have

$$\mathcal{V}(\eta) = \begin{cases} a''/a - U(\eta), & \text{scalar,} \\ a''/a, & \text{tensor.} \end{cases} \quad (4.18)$$

However, as we mentioned above, we can safely ignore the $U(\eta)$ term in the scalar perturbation equation during the bouncing phase. As a result, both scalar and tensor perturbations obey the same equation with the same effective potential a''/a . So, in this subsection we only need to consider one of them during the bouncing phase.

In order to solve the perturbation equation, let us first consider the analytical expression of a''/a . From the analytical equation of $a(t)$ and the relation $dt/a(t) = d\eta$, we find

$$\mathcal{V}(\eta) \equiv \frac{a''}{a} = a_B^2 \frac{\gamma_B m_{\text{Pl}}^2 (3 - \gamma_B t^2/t_{\text{Pl}}^2)}{9(1 + \gamma_B t^2/t_{\text{Pl}}^2)^{5/3}}. \quad (4.19)$$

If we consider Eq. (4.17) as the Schrödinger equation, the term $\mathcal{V}(\eta)$ serves as an effective barrier during the bouncing phase. This potential can be approximated by a PT potential for which we know the analytical solution,

$$\mathcal{V}_{\text{PT}}(\eta) = \frac{\mathcal{V}_0}{\cosh^2 \alpha(\eta - \eta_B)}. \quad (4.20)$$

Here \mathcal{V}_0 is the height of the effective potential and $-2\mathcal{V}_0\alpha^2$ is the curvature of the potential at its maximum. Specifically for $\mathcal{V}(\eta)$ given by Eq. (4.19), one has

$$\mathcal{V}_0 = \frac{a_B^2 \gamma_B m_{\text{Pl}}^2}{3} = k_B^2 = \frac{\alpha^2}{6}. \quad (4.21)$$

In Fig. 19, we plot the PT potential and the one given by Eq. (4.19), from which we can see that $\mathcal{V}_{\text{PT}}(\eta)$ mimics $\mathcal{V}(\eta)$ very well.

To find the analytical solution of Eq. (4.17) with the PT potential, we define two new variables x and $\mathcal{Y}(x)$ via the relations,

$$x(\eta) = \frac{1}{1 + e^{-2\sqrt{6}k_B(\eta - \eta_B)}}, \quad (4.22)$$

$$\mathcal{Y}(x) = [x(1-x)]^{ik/(2\sqrt{6}k_B)} \mu_k(\eta), \quad (4.23)$$

and rewrite Eq. (4.17) as

$$x(1-x) \frac{d^2 \mathcal{Y}}{dx^2} + [a_3 - (a_1 + a_2 + 1)x] \frac{d\mathcal{Y}}{dx} - a_1 a_2 \mathcal{Y} = 0, \quad (4.24)$$

where

$$\begin{aligned} a_1 &\equiv \frac{1}{2} \left(1 + \frac{1}{\sqrt{3}} \right) - \frac{ik}{\sqrt{6} k_B}, \\ a_2 &\equiv \frac{1}{2} \left(1 - \frac{1}{\sqrt{3}} \right) - \frac{ik}{\sqrt{6} k_B}, \\ a_3 &\equiv 1 - \frac{ik}{\sqrt{6} k_B}. \end{aligned} \quad (4.25)$$

Eq. (4.24) is the standard hypergeometric equation, and has the general solution,

$$\begin{aligned} \mu_k^{(\text{PT})}(\eta) &= a_k x^{ik/(2\sqrt{6}k_B)} (1-x)^{-ik/(2\sqrt{6}k_B)} \\ &\times {}_2F_1(a_1 - a_3 + 1, a_2 - a_3 + 1, 2 - a_3, x) \\ &+ b_k [x(1-x)]^{-ik/(2\sqrt{6}k_B)} {}_2F_1(a_1, a_2, a_3, x). \end{aligned} \quad (4.26)$$

Here a_k and b_k are two independent integration constants, and $\alpha = \sqrt{6}k_B$ as given in Eq. (4.21). They are uniquely determined by the initial conditions.

D. Perturbations During the Transition Phase

After the bouncing phase, the kinetic energy of the scalar field ϕ keeps decreasing and the potential energy

soon becomes dominant. As shown in Fig. 18, during this transition phase we have

$$k^2 \gg \left| \frac{a''}{a} - U(\eta) \right|, \quad k^2 \gg \left| \frac{a''}{a} \right|. \quad (4.27)$$

Thus, the equation of motion for both scalar and tensor perturbations can be described by

$$\mu_k''(\eta) + k^2 \mu_k(\eta) = 0, \quad (4.28)$$

which has the general solutions,

$$\mu_k(\eta) = \frac{1}{\sqrt{2k}} \left(\tilde{\alpha}_k e^{-ik\eta} + \tilde{\beta}_k e^{ik\eta} \right), \quad (4.29)$$

where $\tilde{\alpha}_k$ and $\tilde{\beta}_k$ are two constants.

It is remarkable to note that during both, the bouncing and transition phase, the scalar and tensor perturbations obey the same equation of motion. As to be shown below, this is no longer the case during the slow-roll inflationary phase.

E. Perturbations During the Slow-Roll Inflationary Phase

After the transition phase, the energy density dropped down to about $10^{-12} \rho_c$ and the universe enters the slow-roll inflationary phase. During this period, the equations of motion for both scalar and tensor perturbations are relativistic, and can be described by

$$\mu_k''(\eta) + \left(k^2 - \frac{\nu_{s,t}^2 + 1/4}{\eta^2} \right) \mu_k(\eta) = 0, \quad (4.30)$$

where $\nu_{s,t}(\eta)$ can be expressed in terms of the slow-roll parameters and the subscripts “s,t” denote scalar and tensor perturbations, respectively. For the scalar perturbations, we have

$$\nu_s^2 \simeq \eta^2 \frac{z_s''(\eta)}{z_s(\eta)} + \frac{1}{4}, \quad (4.31)$$

with $z_s = a\dot{\phi}/H$, while for the tensor perturbations, we have

$$\nu_t^2 \simeq \eta^2 \frac{z_t''(\eta)}{z_t(\eta)} + \frac{1}{4}, \quad (4.32)$$

with $z_t = a(t)$. As both ν_s and ν_t are the slow-roll quantities during the slow-roll inflation, we can take them as constant approximately. Then, the approximate solutions of Eq. (4.30) can be solved analytically and expressed as a linear combination of Hankel functions,

$$\mu_k^{(s,t)}(\eta) \simeq \frac{\sqrt{-\pi\eta}}{2} \left[\alpha_k H_{\nu_{s,t}}^{(1)}(-k\eta) + \beta_k H_{\nu_{s,t}}^{(2)}(-k\eta) \right], \quad (4.33)$$

where we already ignored the irrelevant phase factor $e^{i(1+2\nu_{s,t})\pi/4}$.

F. Matching the Solutions Together

Now we need to determine the coefficients α_k and β_k by connecting the solutions (4.33), (4.29), and (4.26) together in their intermediate regions. For this purpose, we first consider the limit $\eta - \eta_B \gg 0$ for the solution (4.26), from which we find

$$x \sim 1 - e^{-2\sqrt{6}k_B(\eta - \eta_B)} \rightarrow 1. \quad (4.34)$$

Thus, we obtain

$$1 - x \sim e^{-2\sqrt{6}k_B(\eta - \eta_B)}. \quad (4.35)$$

Using the relations,

$$\begin{aligned} & {}_2F_1(a_1 - a_3 + 1, a_2 - a_3 + 1, 2 - a_3, x) \\ &= (1-x)^{a_3 - a_1 - a_2} \frac{\Gamma(2 - a_3)\Gamma(a_1 + a_2 - a_3)}{\Gamma(a_1 - a_3 + 1)\Gamma(a_2 - a_3 + 1)} {}_2F_1(1 - a_1, 1 - a_2, 1 + a_3 - a_1 - a_2, 1 - x) \\ &+ \frac{\Gamma(2 - a_3)\Gamma(a_3 - a_1 - a_2)}{\Gamma(1 - a_1)\Gamma(1 - a_2)} {}_2F_1(a_1 - a_3 + 1, a_2 - a_3 + 1, a_1 + a_2 - a_3 + 1, 1 - x), \end{aligned} \quad (4.36)$$

and

$$\begin{aligned} {}_2F_1(a_1, a_2, a_3, x) &= (1-x)^{a_3 - a_1 - a_2} \frac{\Gamma(a_3)\Gamma(a_1 + a_2 - a_3)}{\Gamma(a_1)\Gamma(a_2)} {}_2F_1(a_3 - a_1, a_3 - a_2, a_3 - a_1 - a_2 + 1, 1 - x) \\ &+ \frac{\Gamma(a_3)\Gamma(a_3 - a_1 - a_2)}{\Gamma(a_3 - a_1)\Gamma(a_3 - a_1)} {}_2F_1(a_1, a_2, a_1 + a_2 + 1 - a_3, 1 - x), \end{aligned} \quad (4.37)$$

we find

$$\mu_k^{\text{PT}}(\eta) = \left[a_k \frac{\Gamma(2 - a_3)\Gamma(a_1 + a_2 - a_3)}{\Gamma(a_1 - a_3 + 1)\Gamma(a_2 - a_3 + 1)} + b_k \frac{\Gamma(a_3)\Gamma(a_1 + a_2 - a_3)}{\Gamma(a_1)\Gamma(a_2)} \right] e^{-ik(\eta - \eta_B)}$$

$$+ \left[a_k \frac{\Gamma(2-a_3)\Gamma(a_3-a_1-a_2)}{\Gamma(1-a_1)\Gamma(1-a_2)} + b_k \frac{\Gamma(a_3)\Gamma(a_3-a_1-a_2)}{\Gamma(a_3-a_1)\Gamma(a_3-a_2)} \right] e^{ik(\eta-\eta_B)}. \quad (4.38)$$

Comparing Eqs. (4.38) and (4.29), we obtain,

$$\frac{\tilde{\alpha}_k}{\sqrt{2k}} = \left[a_k \frac{\Gamma(2-a_3)\Gamma(a_1+a_2-a_3)}{\Gamma(a_1-a_3+1)\Gamma(a_2-a_3+1)} + b_k \frac{\Gamma(a_3)\Gamma(a_1+a_2-a_3)}{\Gamma(a_1)\Gamma(a_2)} \right] e^{ik\eta_B}, \quad (4.39)$$

$$\frac{\tilde{\beta}_k}{\sqrt{2k}} = \left[a_k \frac{\Gamma(2-a_3)\Gamma(a_3-a_1-a_2)}{\Gamma(1-a_1)\Gamma(1-a_2)} + b_k \frac{\Gamma(a_3)\Gamma(a_3-a_1-a_2)}{\Gamma(a_3-a_1)\Gamma(a_3-a_2)} \right] e^{-ik\eta_B}. \quad (4.40)$$

Then, considering the solution (4.33) in the limit $-k\eta \rightarrow \infty$, we obtain

$$\mu_k(\eta) = \frac{\alpha_k}{\sqrt{2k}} e^{-ik\eta} + \frac{\beta_k}{\sqrt{2k}} e^{ik\eta}. \quad (4.41)$$

Comparing it with Eq. (4.29), we find

$$\begin{aligned} \frac{\alpha_k}{\sqrt{2k}} &= \frac{\tilde{\alpha}_k}{\sqrt{2k}} \\ &= \left[a_k \frac{\Gamma(2-a_3)\Gamma(a_1+a_2-a_3)}{\Gamma(a_1-a_3+1)\Gamma(a_2-a_3+1)} + b_k \frac{\Gamma(a_3)\Gamma(a_1+a_2-a_3)}{\Gamma(a_1)\Gamma(a_2)} \right] e^{ik\eta_B}, \end{aligned} \quad (4.42)$$

$$\begin{aligned} \frac{\beta_k}{\sqrt{2k}} &= \frac{\tilde{\beta}_k}{\sqrt{2k}} \\ &= \left[a_k \frac{\Gamma(2-a_3)\Gamma(a_3-a_1-a_2)}{\Gamma(1-a_1)\Gamma(1-a_2)} + b_k \frac{\Gamma(a_3)\Gamma(a_3-a_1-a_2)}{\Gamma(a_3-a_1)\Gamma(a_3-a_2)} \right] e^{-ik\eta_B}. \end{aligned} \quad (4.43)$$

Now several comments are in order:

- Since a_i 's depend on k/k_B via Eq. (4.25), we can see that α_k and β_k in general also depend on k/k_B .
- In general relativity, the BD vacuum is normally imposed [4],

$$\alpha_k^{\text{GR}} = 1, \quad \beta_k^{\text{GR}} = 0, \quad (4.44)$$

whenever the mode is inside the Hubble horizon. When the effects of the pre-inflationary dynamics are taken into account, in general this is no longer the case. In fact, both of them now depend on the constants a_k and b_k , which are closely related to the pre-inflationary dynamics during the bouncing phase.

- The quantity $|\beta_k|^2$ represents the rate of particle creation due to the expansion of the universe. In general β_k does not vanish, that is, particles are generically created due to the expansion of the universe during the bouncing and transition phases.

- Eqs. (4.42) and (4.43) are valid for both scalar and tensor perturbations. Thus, if the same initial conditions are chosen for these two types of perturbations, the effects of pre-inflationary dynamics are also the same. This is a *unique characteristic of the dressed metric approach*.

Now with the analytical solution of Eq. (4.33) and α_k and β_k given by Eqs. (4.42) and (4.43), let us turn to compute the power spectra for both scalar and tensor perturbations. For the scalar perturbations, the primordial power spectrum can be calculated in the limit $-k\eta \rightarrow 0^+$, and is given by,

$$\mathcal{P}_{\mathcal{R}}(k) \equiv \frac{k^3}{4\pi^2} |\mathcal{R}_k(\eta)|^2 = \frac{k^3}{4\pi^2} \left| \frac{\mu_k^{(s)}(\eta)}{z_s(\eta)} \right|^2. \quad (4.45)$$

Using the asymptotic form of the Hankel functions,

$$\lim_{-k\eta \rightarrow 0^+} H_\nu^{(1,2)}(-k\eta) \simeq \mp \frac{i}{\pi} \Gamma(\nu) \left(\frac{-k\eta}{2} \right)^{-\nu}, \quad (4.46)$$

where $+$, $-$ correspond to $H_\nu^{(2)}(-k\eta)$ and $H_\nu^{(1)}(-k\eta)$ respectively, we find

$$\mu_k^{(s)}(\eta) \rightarrow i \sqrt{\frac{-\eta}{2\pi}} (\alpha_k + \beta_k) \Gamma(\nu_s) \left(\frac{-k\eta}{2} \right)^{-\nu_s}. \quad (4.47)$$

Then, the power spectrum reads

$$\mathcal{P}_{\mathcal{R}}(k) = |\alpha_k + \beta_k|^2 \mathcal{P}_{\mathcal{R}}^{\text{GR}}(k), \quad (4.48)$$

where

$$\mathcal{P}_{\mathcal{R}}^{\text{GR}}(k) \equiv \frac{k^2}{4\pi^3} \left(\frac{H}{a\dot{\phi}} \right)^2 \Gamma^2(\nu_s) \left(\frac{-k\eta}{2} \right)^{1-2\nu_s}, \quad (4.49)$$

is the standard inflationary scalar spectrum for a single scalar field inflationary model in GR, and α_k and β_k are given by Eqs. (4.42) and (4.43) in terms of a_k and b_k . The latter are determined by the initial conditions.

Note that Eq. (4.48) is *the most general expression for the scalar power spectrum in the framework of the dressed metric approach in LQC*. Once the initial conditions are specified, it will be uniquely determined.

In addition, as mentioned above, α_k and β_k depend on the comoving wavenumber k via the coefficients a_i 's through Eq. (4.25), so the power spectrum $\mathcal{P}_{\mathcal{R}}(k)$ is generically scale-dependent, due to the quantum gravitational effects. Clearly, to be consistent with observations

[6, 7], which show that the power spectrum is almost scale-invariant, the dependence cannot be strong. Otherwise, it will be inconsistent with observations. Such a dependence clearly is closely related to the initial conditions, which will be considered in detail in the next section. For some given initial conditions, observations will impose strong constraints on the effects of pre-inflationary dynamics, which will provide an excellent opportunity to test observationally the theory of LQC, or more precisely, the ideas of the dressed metric approach.

For the tensor perturbation, the primordial power spectrum of $h = 2M_{\text{Pl}}\mu_k^{(t)}(\eta)/a(\eta)$ can be calculated in the limit $-k\eta \rightarrow 0^+$ via the expression,

$$\mathcal{P}_h \equiv \frac{k^3}{4\pi^2} |h(k)|^2 = \frac{k^3}{4\pi^2} \left| \frac{2\mu_k^{(t)}(\eta)}{M_{\text{Pl}}a(\eta)} \right|^2. \quad (4.50)$$

Similar to the scalar case, using the asymptotic form of the Hankel functions given by Eq. (4.33) in the limit $-k\eta \rightarrow 0^+$, we find

$$\mu_k^{(t)}(\eta) \rightarrow i\sqrt{\frac{-\eta}{2\pi}}(\alpha_k + \beta_k)\Gamma(\nu_t) \left(\frac{-k\eta}{2}\right)^{-\nu_t}. \quad (4.51)$$

Then, the tensor spectrum reads

$$\mathcal{P}_h(k) = |\alpha_k + \beta_k|^2 \mathcal{P}_h^{\text{GR}}(k), \quad (4.52)$$

where

$$\mathcal{P}_h^{\text{GR}}(k) \equiv \frac{k^2}{\pi^3 M_{\text{Pl}}^2 a^2} \Gamma^2(\nu_t) \left(\frac{-k\eta}{2}\right)^{1-2\nu_t}, \quad (4.53)$$

and α_k and β_k are given by Eqs. (4.42) and (4.43), which are generically scale-dependent, as mentioned above. Once the initial conditions are given, they are uniquely determined. Eq. (4.52) is *the most general expression for the tensor power spectrum in the framework of the dressed metric approach in LQC, and in general depends on the comoving wavenumber k , due to the quantum gravitational effects during the pre-inflationary phases.*

It should be noted that the corrections due to the quantum gravitational effects of the pre-inflationary dynamics are all proportional to the factor $|\alpha_k + \beta_k|^2$ for both scalar and tensor perturbations, as one can see from Eqs. (4.48) and (4.52). As mentioned above, if the same initial conditions for these two types of perturbations are imposed, for example, all of them are in the Bunch-Davies vacuum initially, this factor will be the same. Then, the ratio r between the scalar and tensor perturbations remains the same as that given in GR!

V. INITIAL CONDITIONS AND EFFECTS OF PRE-INFLATIONARY DYNAMICS IN PRIMORDIAL SPECTRA

In the last section, the linear cosmological perturbations were calculated in each of the three phases prior to preheating, i.e., the bouncing, transition and slow-roll

inflationary phases [cf. Figs. 15 and 18], and analytical expressions of the mode functions for both scalar and tensor perturbations were found, whereby the corresponding power spectra were computed and given explicitly by Eqs. (4.48) and (4.52). The mode functions found in these three different phases were also matched together and finally given by Eqs. (4.42) and (4.43), in which the parameters α_k and β_k of the mode functions in the slow-roll inflationary phase are expressed as functions of a_k and b_k of the mode functions in the bouncing phase. The latter will be determined by initial conditions. So, in this section, we shall first consider the initial conditions, and then we study the effects of the quantum bounce and its subsequent pre-inflationary dynamics during the bouncing and transition phase on the power spectra.

A. Initial Conditions of Primordial Perturbations

In the framework of LQC, various sets of initial conditions have been investigated [38, 55, 62–69]. However, this is a subtle issue, because in general there is not a preferred initial state for a quantum field in arbitrarily curved space-times. If the universe is sufficiently spatially flat and evolves sufficiently slowly so that the characteristic scale for a perturbation mode is much larger than its wavelength, there is an approximate definition of the initial state: the Bunch-Davies vacuum state. This is also the common initial state adopted in general relativity at the beginning of the slow-roll inflation where all the relevant perturbation modes are well inside the Hubble horizon [4].

However, in the pre-inflationary phases, especially near the bounce, the background geometry is far from the slow-roll inflationary phase. In particular, for the perturbations during the bouncing phase, as illustrated in Fig. 18, their wavelengths could be larger, equal, or smaller than the corresponding characteristic scale. Thus, it is in general impossible to assume that the universe is in the Bunch-Davies vacuum at the bounce [62, 66, 67]. In this subsection, we consider only two of them that have been frequently used in the literature, and show that they essentially lead to the same results.

1. The BD Vacuum in Contracting Phase

As illustrated in Fig. 18, during the contracting phase right before the bounce, all the relevant perturbation modes are well inside the characteristic length λ . Then, we can naturally choose the BD vacuum state as the initial conditions of the perturbations of both scalar and tensor [65],

$$\mu_k^{\text{initial}}(\eta) \sim \frac{1}{\sqrt{2k}} e^{-ik\eta}, \quad (5.1)$$

with which we can uniquely determine the coefficients a_k and b_k appearing in Eqs. (4.42) and (4.43). Considering

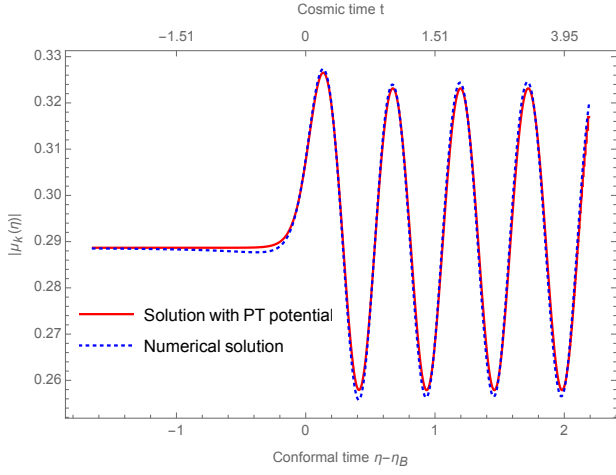


FIG. 20. Comparison between the analytical solution given by Eq. (4.26) and the numerical solution with the initial condition (5.4), $a_B = 1$, and $m_{P1} = 1$.

that during the contracting phase, we have $\eta - \eta_B \ll 0$, we find

$$x \sim e^{2\sqrt{6}k_B(\eta - \eta_B)} \rightarrow 0, \quad (5.2)$$

and thus

$$\begin{aligned} x^{ik/(2\sqrt{6}k_B)}(1-x)^{-ik/(2\sqrt{6}k_B)} &\sim e^{ik(\eta - \eta_B)}, \\ (x(1-x))^{-ik/(2\sqrt{6}k_B)} &\sim e^{-ik(\eta - \eta_B)}. \end{aligned} \quad (5.3)$$

Inserting the above expressions into Eq. (4.26), and then comparing it with the above initial condition, we find that,

$$a_k = 0, \quad b_k = \frac{e^{ik\eta_B}}{\sqrt{2k}}. \quad (5.4)$$

Note that in the above calculations we used the fact ${}_2F_1(c_1, c_2, c_2, 0) = 1$. Fig. 20 shows our analytical solution together with the numerical one, from which we can see that they match extremely well during the bouncing phase.

Here we would like to note that most of the modes (with $k^2 \gg |a''/a|$) are well inside the characteristic length λ during the contracting phase. As a result, $\mu_k^{\text{PT}}(\eta)$ of Eq. (4.26) with the initial condition of the BD vacuum state imposed at the contracting phase are valid for all these modes, even if some of them (with $k < k_B$) are outside the characteristic length λ at the bounce.

2. The Fourth-order Adiabatic Vacuum State at the Bounce

Another moment of the initial conditions is right at the bounce [38]. However, as we mentioned above, at this point the curvature of the background geometry has significant effects on the perturbation modes. This is different from the case of the quasi-de-Sitter spacetime or the contracting phase right before the bounce. Therefore,

it is not possible to impose the BD vacuum state at the bounce.

Instead, one can impose two conditions, *the adiabatic regularization* and *maximal symmetry* of the perturbation modes, with which it was shown [16–18, 66] that the state of the perturbations at the bounce can be constructed as *the fourth-order adiabatic vacuum*. According to [18], the fourth-order adiabatic vacuum of Eq. (4.17) with $V(\eta)$ being given by Eq. (4.18) can be written in the form

$$\mu_k(\eta) = \frac{1}{\sqrt{2W_k^{(4)}(\eta)}} e^{-i \int^\eta W_k^{(4)}(\bar{\eta}) d\bar{\eta}}, \quad (5.5)$$

where

$$W_k^{(4)}(\eta) = \sum_{i=1}^{i=4} W_i, \quad (5.6)$$

with

$$W_0 = k, \quad (5.7)$$

$$W_1 = 0, \quad (5.8)$$

$$W_2 = -\frac{1}{2k} \frac{a''}{a}, \quad (5.9)$$

$$W_3 = 0, \quad (5.10)$$

$$W_4 = \frac{1}{8k^3} \left(\frac{2a''a'^2}{a^3} - \frac{2a''^2}{a^2} - \frac{2a'a''''}{a^2} + \frac{a'''''}{a} \right). \quad (5.11)$$

The above state is constructed from the generalized WKB approximate solution of the fourth-order and can also be regarded as an expansion in the number of derivatives of the scale factor. The leading order in the expansion corresponds to the positive energy solution in the Minkowski space and the rest of the terms are higher-order contributions that vanish at different rates when $a/k \rightarrow 0$ [17, 18].

Here we would like to note that, as also pointed out in [17, 18], 2. This implies that the fourth-order adiabatic vacuum state constructed above can only apply to the modes with $k \geq k_B$, here k_B represents the maximum value of $\sqrt{a''/a}$ during the bouncing phase [c.f. Fig. 18]. For the modes with $k < k_B$, as pointed out in [17, 18], ambiguity remains in constructing the vacuum state at the bounce.

Imposing *the fourth-order adiabatic vacuum* at the bounce for modes with $k \geq k_B$, we find

$$W_2 = -\frac{a_B^2 \gamma_B}{6kt_{P1}^2} = -\frac{k_B^2}{2k}, \quad (5.12)$$

$$W_4 = -\frac{13a_B^4 \gamma_B^2}{72k^3 t_{P1}^4} = -\frac{13k_B^4}{8k^3}. \quad (5.13)$$

Using these results and expanding the fourth-order adiabatic vacuum state up to the order of $O(k_B^4/k^4)$, we find

$$\mu_k(\eta_B) = \frac{1}{\sqrt{2k}} \left[1 - \frac{1}{4} \frac{k_B^2}{k^2} - \frac{29}{32} \frac{k_B^4}{k^4} + \mathcal{O}\left(\frac{k_B^6}{k^6}\right) \right].$$

$$(5.14)$$

Now we are in the position to determine the coefficients a_k and b_k appearing in Eq. (4.26) by connecting the initial state with the analytical solution (4.26) at the bounce, at which we find

$$\begin{aligned} \mu^{(\text{PT})}(\eta_{\text{B}}) &= a_k {}_2F_1\left(\frac{1-\sqrt{3}}{2}, \frac{1+\sqrt{3}}{2}, 1 + \frac{ik}{\sqrt{6}k_{\text{B}}}, \frac{1}{2}\right) \\ &+ b_k \sqrt{\pi} 4^{\frac{ik}{2\sqrt{6}k_{\text{B}}}} \Gamma\left(1 - \frac{ik}{\sqrt{6}k_{\text{B}}}\right) \\ &\times \Gamma^{-1}\left(\frac{3}{4} - \frac{\sqrt{3}}{12} - \frac{ik}{2\sqrt{6}k_{\text{B}}}\right) \\ &\times \Gamma^{-1}\left(\frac{3}{4} + \frac{\sqrt{3}}{12} - \frac{ik}{2\sqrt{6}k_{\text{B}}}\right). \end{aligned} \quad (5.15)$$

Then, using the asymptotic expansions of the Gamma function appearing in Eq. (B.13) of Appendix B, we arrive at the same results of Eq. (5.4). Note that in obtaining the above result, we had simply ignored an irrelevant phase difference between (5.15) and (5.14).

Thus, we conclude that the solution of Eq. (4.26) starting with a BD vacuum state at the contracting phase will reduce to the one obtained by imposing *the fourth-order adiabatic vacuum state* at the bounce. This is easy to understand. In fact, if one applies *the fourth-order adiabatic vacuum state* to Eq. (5.5) at the contracting phase, one can see that the perturbation modes also satisfy the BD vacuum condition there. However, it must be noted that the perturbations with the BD vacuum initial condition and the fourth-order adiabatic vacuum one are the same only for the modes with $k \geq k_{\text{B}}$. For other modes, *the fourth-order adiabatic vacuum state* at the bounce is not applicable, while the BD vacuum initial state can be still applied to these modes but in the contracting phase.

B. Effects of the Pre-inflationary Dynamics on Primordial Power Spectra

With the coefficients a_k and b_k being given by Eq. (5.4), the coefficients α_k and β_k appearing in Eqs. (4.42) and (4.43) can be casted in the form

$$\begin{aligned} \alpha_k &= \frac{\Gamma(a_3)\Gamma(a_1+a_2-a_3)}{\Gamma(a_1)\Gamma(a_2)} e^{2ik\eta_{\text{B}}}, \\ \beta_k &= \frac{\Gamma(a_3)\Gamma(a_3-a_1-a_2)}{\Gamma(a_3-a_1)\Gamma(a_3-a_2)}. \end{aligned} \quad (5.16)$$

Then, we find that

$$\begin{aligned} |\alpha_k + \beta_k|^2 &= 1 + \left[1 + \cos\left(\frac{\pi}{\sqrt{3}}\right)\right] \text{csch}^2\left(\frac{\pi k}{\sqrt{6}k_{\text{B}}}\right) \\ &+ \sqrt{2} \sqrt{\cosh\left(\frac{2\pi k}{\sqrt{6}k_{\text{B}}}\right) + \cos\left(\frac{\pi}{\sqrt{3}}\right)} \cos\left(\frac{\pi}{2\sqrt{3}}\right) \end{aligned}$$

$$\times \text{csch}^2\left(\frac{\pi k}{\sqrt{6}k_{\text{B}}}\right) \cos(2k\eta_{\text{B}} + \varphi_k), \quad (5.17)$$

where

$$\varphi_k \equiv \arctan\left\{\frac{\text{Im}[\Gamma(a_1)\Gamma(a_2)\Gamma^2(a_3-a_1-a_2)]}{\text{Re}[\Gamma(a_1)\Gamma(a_2)\Gamma^2(a_3-a_1-a_2)]}\right\}. \quad (5.18)$$

In Fig. 21 we display the ratio between the power spectrum with the bouncing effects and the standard one given in GR, as a function of the wave-number k . We would like to note that Fig. 21 is consistent with the one presented in [16, 18] [c.f. Fig. 1 in [16] and Fig. 5 in [18]]. While the results obtained in [16, 18] are purely numerical, here our results are derived directly from the analytical expression given by Eq. (5.17).

It is remarkable to note that *the pre-inflationary dynamics leads to oscillations in the power spectra of both scalar and tensor perturbations, and the amplitudes of these oscillations are independent of the slow-roll inflationary models, although they depend explicitly on k* . The amplitudes of these oscillations, which essentially depend on the parameter $\alpha[= \sqrt{6}k_{\text{B}}]$, represent a characteristic feature of LQC. In Eq. (5.17), the last two terms, proportional to $\text{csch}^2(\pi k/(\sqrt{6}k_{\text{B}}))$, decrease exponentially as k increases. In other words, the power spectra get reduced exponentially for $k/k_{\text{B}} \gg 1$. However, as $k/k_{\text{B}} \simeq 0$, they get enhanced as $(k_{\text{B}}/k)^2$. Hence, the quantum gravitational effects are important at the scales $k \lesssim k_{\text{B}}$. These modes, as we mentioned above, are essentially the ones whose energies are of the Planck scale at the bounce. They are initially inside the radius defined by $\lambda = \sqrt{|a/a''|}$, and then leave and re-enter it during the bouncing phase. The modes with $k \gg k_{\text{B}}$ are always inside the radius before they leave the Hubble horizon during the slow-roll inflationary phase, thus finally they lead to a standard power-law spectrum.

Note that the solution with the PT potential is not a good approximation for the modes with a very small wavenumber (i.e., $k^2 \ll |a''/a|$) during the whole bouncing phase). For these modes, if we ignore the k^2 term in Eq. (4.9), the solution can be approximated by

$$\mu_k(\eta) \simeq a_k a(\eta) + b_k/a(\eta), \quad (k^2 \ll |a''/a|), \quad (5.19)$$

which has been considered in detail in [44]. However, these modes are beyond our interest because they are still outside of our currently observable universe.

VI. OBSERVATIONAL CONSTRAINTS ON THE EFFECTS OF THE PRE-INFLATIONARY DYNAMICS

The quantum corrections (5.17) are k -dependent and expected to be constrained by observations. In the following, we perform the CMB likelihood analysis by using the Planck 2015 data [7], with the MCMC code developed in [70]. In order to carry out the CosmoMC code let us

TABLE V. Best fit values of the six cosmological parameters and the constraints on k_B/a_0 and r at 95% C.L for different cosmological models from different data combinations.

Parameter	Planck TT+lowP	Planck TT,TE,EE+lowP	Planck TT+lowP+r	Planck TT,TE,EE+lowP+r
$\Omega_b h^2$	0.022355	0.022193	0.022322	0.022064
$\Omega_c h^2$	0.11893	0.12000	0.11908	0.12071
$100\theta_{MC}$	1.04115	1.04065	1.04080	1.04057
τ	0.077835	0.089272	0.081955	0.085259
$\ln(10^{10}A_s)$	3.088	3.112	3.101	3.104
n_s	0.9662	0.9647	0.9658	0.9607
k_B/a_0	$< 3.12 \times 10^{-4}$	$< 3.05 \times 10^{-4}$	$< 3.14 \times 10^{-4}$	$< 3.14 \times 10^{-4}$
r	-----	---	< 0.113	< 0.107

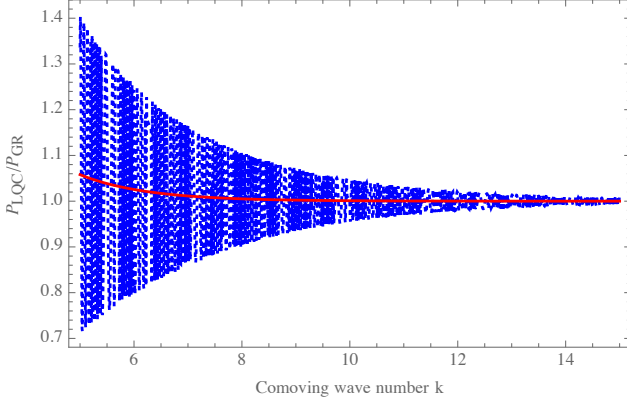


FIG. 21. Ratio between the power spectrum with the effects of the pre-inflationary dynamics and the standard power-law spectrum obtained in GR. The dotted blue curve denotes the analytical power spectrum given by Eq. (5.17), which obviously oscillates rapidly with k . The solid red curve shows the average of the oscillating spectrum.

parameterize the primordial scalar and tensor spectra described in Eqs. (4.48) and (4.52) as,

$$\mathcal{P}_{\mathcal{R}}(k) = (1 + \delta_{\text{PI}})\mathcal{P}_{\mathcal{R}}^{\text{GR}}(k), \quad (6.1)$$

$$\mathcal{P}_h(k) = (1 + \delta_{\text{PI}})\mathcal{P}_h^{\text{GR}}(k), \quad (6.2)$$

where δ_{PI} is given by ²

$$\delta_{\text{PI}} = \left[1 + \cos\left(\frac{\pi}{\sqrt{3}}\right) \right] \text{csch}^2\left(\frac{\pi k}{\sqrt{6}k_B}\right), \quad (6.3)$$

and the standard power-law spectra $\mathcal{P}_{\mathcal{R}}^{\text{GR}}(k)$ and $\mathcal{P}_h^{\text{GR}}(k)$ are parameterized in their standard forms,

$$\begin{aligned} \mathcal{P}_{\mathcal{R}}^{\text{GR}} &= A_s \left(\frac{k}{k_*}\right)^{n_s-1+\dots}, \\ \mathcal{P}_h^{\text{GR}} &= A_t \left(\frac{k}{k_*}\right)^{n_t+\dots}. \end{aligned} \quad (6.4)$$

² The oscillating terms in Eq. (5.17) oscillate very fast and have negligible effects when integrating them out with time. So, they can be safely ignored observationally. In addition, in [57] δ_{PI} was denoted by $\delta_{\mathcal{P}}$.

Here $A_s(A_t)$ is the scalar (tensor) amplitude, $n_s(n_t)$ the scalar (tensor) spectral index, and $k_* = 0.05\text{Mpc}^{-1}$ denotes the pivot scale.

We assume the flat cold dark matter model with the effective number of neutrinos $N_{\text{eff}} = 3.046$ and fix the total neutrino mass $\Sigma m_\nu = 0.06\text{eV}$. Let us first consider the scalar spectrum and vary the following seven parameters,

$$(\Omega_b h^2, \Omega_c h^2, \tau, \Theta_s, n_s, A_s, k_B/a_0), \quad (6.5)$$

where $\Omega_b h^2$ and $\Omega_c h^2$ are, respectively, the baryon and cold dark matter densities, τ is the optical depth to reionization, Θ_s is the ratio (multiplied by 100) of the sound horizon at decoupling to the angular diameter distance to the last scattering surface. In addition, we have one more parameter k_B/a_0 , which is related to the effects of the pre-inflationary dynamics. For the six cosmological parameters $(\Omega_b h^2, \Omega_c h^2, \tau, \Theta_s, n_s, A_s)$, we use the same prior ranges as in [71], while for the parameter k_B/a_0 , which is related to the bouncing effects, we set the prior range as $k_B/a_0 \in [10^{-8}, 0.002]\text{Mpc}^{-1}$.

In particular, we use the high- l CMB temperature power spectrum (TT) and the polarization data (TT, TE, EE) respectively with low- l polarization data (lowP) from Planck2015. In Table. V, we list the best fit values of the six cosmological parameters and constraints on k_B/a_0 and r at 95% C.L. for different cosmological models from different data combinations. Marginalizing other parameters, we find that k_B/a_0 is constrained by the Planck TT+lowP (Planck TT,TE,EE+lowP) to [cf. the left panel of Fig. 22],

$$\frac{k_B}{a_0} < 3.12 \times 10^{-4}\text{Mpc}^{-1} (3.05 \times 10^{-4}), \quad \text{at 95\% C.L.} \quad (6.6)$$

When we add one more parameter, the tensor-to-scalar ratio $r = A_{(t)}/A_{(s)}$, to include the tensor spectrum, the Planck TT+lowP (Planck TT,TE,EE+lowP) data yields [cf. the right panel of Fig. 22],

$$\frac{k_B}{a_0} < 3.14 \times 10^{-4}\text{Mpc}^{-1} (3.14 \times 10^{-4}), \quad \text{at 95\% C.L.} \quad (6.7)$$

These upper bounds shows that the observational constraints on the pre-inflationary dynamics effects are robust to different data sets (without/with polarization

data included) and whether the tensor spectrum is included.

In Fig. 23 we show constraints on various pairs of the cosmological parameters and their respective probability distributions for the CosmoMC runs described above and for the results from Planck 2015 data. We notice that the colored curves which represent the probability distributions of k_B/a_0 are almost perfectly superposed, which strongly indicates again that the constraints on k_B derived in this paper are robust.

Using the relation

$$\frac{k_B}{a_0} = \sqrt{\frac{\gamma_B}{3}} \frac{a_B}{a_0} m_{\text{Pl}} = \sqrt{\frac{\gamma_B}{3}} m_{\text{Pl}} e^{-N_{\text{tot}}}, \quad (6.8)$$

where $N_{\text{tot}} \equiv \ln(a_0/a_B)$ denotes the total e-folds from the quantum bounce until today, the above upper bounds on k_B/a_0 can be translated into the constraint on the total e-folds N_{tot} as

$$N_{\text{tot}} > 141 \quad (95\% \text{C.L.}), \quad (6.9)$$

where we have taken $\rho_c = 0.41 m_{\text{Pl}}^4$. This in turn leads to a lower bound $\delta N_* > N_{\text{tot}} - N_* - N_{\text{after}}$, where $\delta N_* \equiv \ln(a_*/a_B)$, $N_* \equiv \ln(a_{\text{end}}/a_*)$, and $N_{\text{after}} \equiv \ln(a_0/a_{\text{end}})$, where a_* denotes the expansion factor at the moment that our current horizon exited the Hubble horizon during the slow-roll inflation, and a_{end} is that at the end of inflation. Taking $N_* \simeq 60 \simeq N_{\text{after}}$, we find

$$\delta N_* \gtrsim 21. \quad (6.10)$$

It should be noted that our above results are based on the hypothesis: (1) The universe is filled with a scalar field with an inflationary potential $V(\phi)$ and the background evolution is dominated by the kinetic energy of the inflaton at the quantum bounce. (2) We impose the BD vacuum initial conditions at the contracting phase right before the quantum bounce.

VII. SUMMARY AND OURLOOK

In this paper, we have provided a detailed and systematic study of the evolutions of the background and linear scalar and tensor perturbations of a flat FLRW universe in the framework of *the dressed metric approach* of LQC [16–18]. A remarkable feature is the replacement of the big bang singularity by a quantum bounce [16–18]. In addition, slow-roll inflation is an attractor in the phase space of the initial conditions and most likely to happen with generic initial conditions [55, 56].

To study the universal properties of the pre-inflationary dynamics in the framework of *the dressed metric approach*, in this paper we have mainly focused on models, the dynamics of which is dominated by the kinetic energy of the inflaton at the quantum bounce, i.e.,

$$\frac{1}{2} \dot{\phi}^2(t_B) \gg V(\phi(t_B)), \quad (7.1)$$

as these models are the only ones found so far that inevitably lead to the slow-roll inflation in the late stage of the evolution of the universe [30, 31].

A. Evolution of the Background

For all the models that satisfy the initial condition (7.1), we have found the following for the evolution of the background of the flat FLRW universe:

- The evolution of the universe prior to the preheating can be divided universally into three different phases (see Fig. 15):

bouncing, transition, and slow-roll inflation.

During the bouncing phase, the evolution of the universe is dominated by the kinetic energy of the inflaton, so the equation of state $w(\phi)$ defined by Eq. (2.11) remains practically $w(\phi) \simeq 1$ during this whole phase. However, at $t/t_{\text{Pl}} \simeq 10^4 \sim 10^5$, the kinetic energy suddenly decreases, and $w(\phi)$ soon decreases from $w(\phi) \simeq 1$ to $w(\phi) \simeq -1$. This transition phase is very short in comparison with the other two phases. Afterwards, the universe enters an accelerating phase, where $\ddot{a} > 0$. At the beginning of this phase, the absolute value of the slow-roll parameter ϵ_H defined by Eq. (2.12) is still large, but soon settles down to zero, whereby the slow-roll inflation starts, as shown explicitly in Section II.

- During the bouncing phase, *the evolutions of the expansion factor $a(t)$ and the scalar field ϕ are independent of the inflationary potential, and can well be approximated by the analytical solutions of Eq. (3.4) and (3.6), respectively.*

The main reason is that the potential $V(\phi)$ remains very small and the kinetic energy is dominant during this whole phase. For example, for the potential $V(\phi) = V_0 \phi^2$, we find that $V(\phi)/m_{\text{Pl}}^4 \in (2 \times 10^{-11}, 4.5 \times 10^{-11})$; for $n = 1/3$, $V(\phi)/m_{\text{Pl}}^4 \in (9 \times 10^{-12}, 1.2 \times 10^{-11})$; and for the Starobinsky potential, we have $V(\phi)/m_{\text{Pl}}^4 \in (7 \times 10^{-13}, 7.3 \times 10^{-13})$. Clearly, in this whole phase, we can safely ignore the effects of the potential and set it to zero, such that the solution Eq.(3.4) for $a(t)$ immediately follows.

- During the transition phase, the expansion factor $a(t)$ and scalar field $\phi(t)$ can be well approximated analytically by Eq. (3.19) with a_c , ϕ_c and $\dot{\phi}_c$ being given by Eqs. (3.14)–(3.16), where t_c is the moment when the kinetic energy is equal to the potential energy, so that $w(\phi_c) = 0$ [cf. Fig. 15]. Then, the e-folds $N_c [\equiv \ln(a_c/a_B)]$ can be calculated analytically by Eq. (3.17).

From the moment t_c until the beginning of the slow-roll inflationary phase, denoted by the time t_i , the

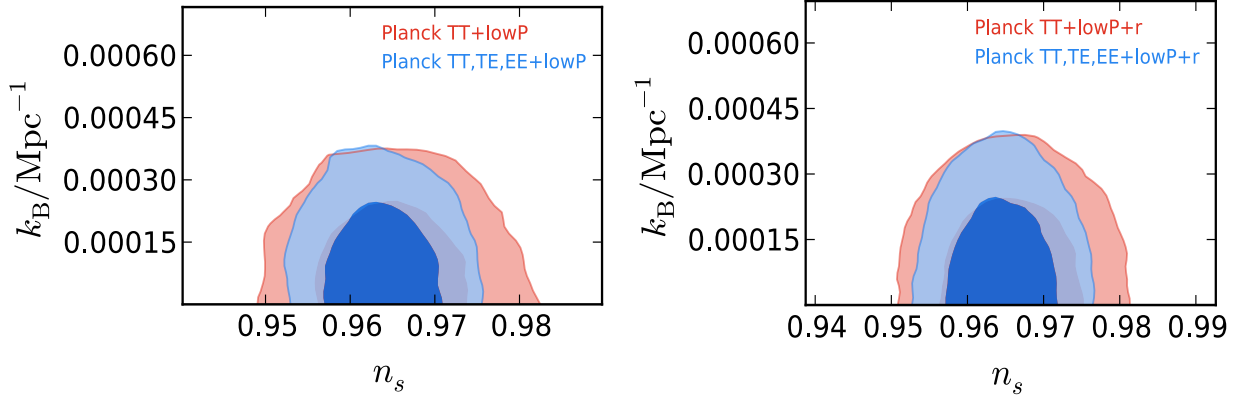


FIG. 22. The CMB likelihood analysis in the (k_B, n_s) -plane with a robust fitting $n_s \simeq 0.965$. The observational constraints on $(n_s, k_B/\text{Mpc}^{-1})$ are obtained at 68% and 95% C.L. by using Planck 2015 TT+lowP and TT, TE, EE+lowP data. The upper panel only considers the scalar spectrum, while the bottom one includes the non-zero tensor contributions. Note that we set $a_0 = 1$.

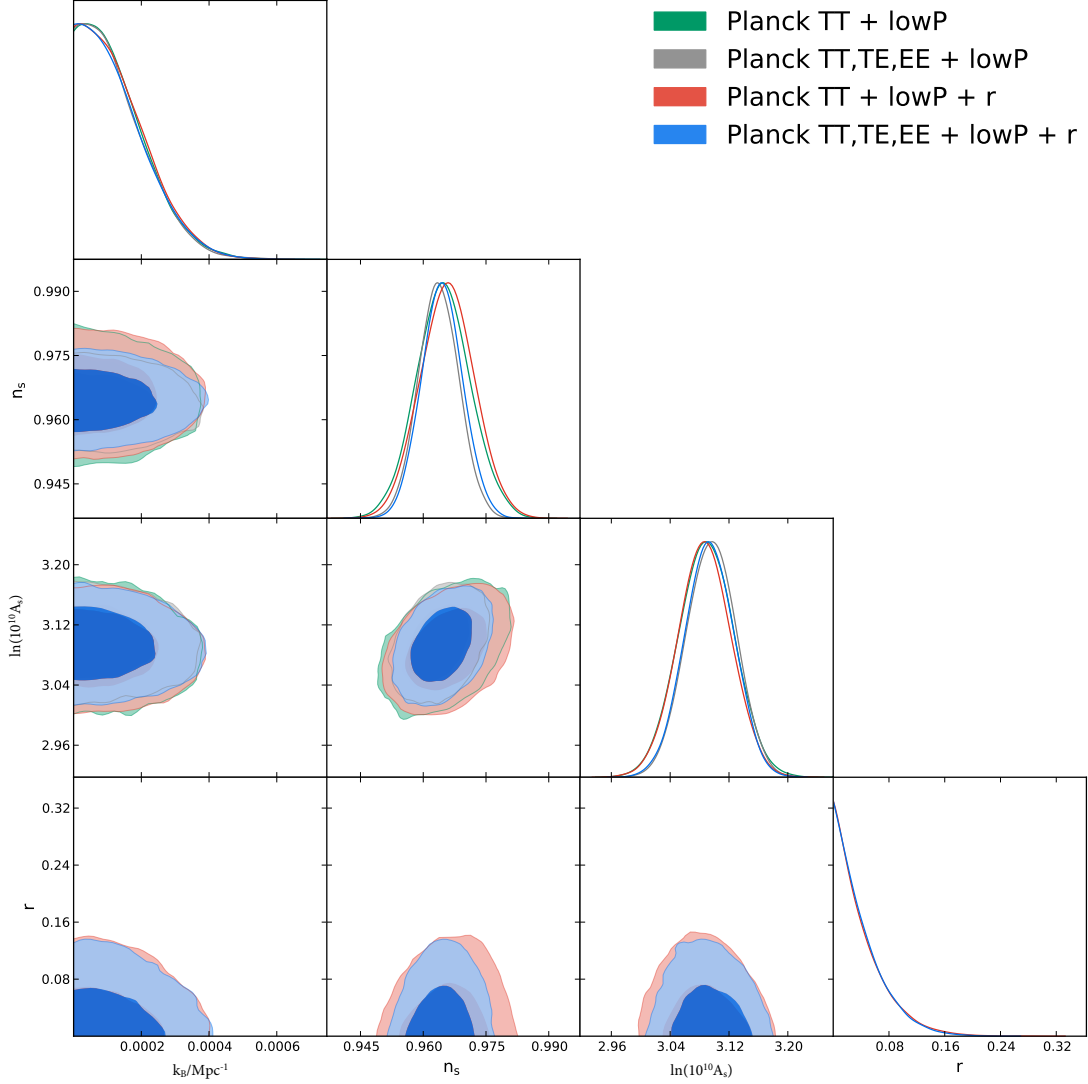


FIG. 23. Observational constraints on various pairs of parameters (68% and 95% contour lines) and the probability distributions for $\ln(10^{10} A_s)$, n_s , k_B/a_0 , and r by using Planck 2015 data. Note that in the numerical simulations we set $a_0 = 1$.

e-fold that the universe expands is $\Delta N \equiv N_i - N_c = \ln(a_i/a_c) \simeq 0.1$, as shown both numerically and analytically in Tables I-IV, where N_i is analytically given by Eq. (3.30).

Once the universe enters the slow-roll inflationary phase, the e-folds $N_{\text{inf}}[\equiv \ln(a_{\text{end}}/a_i)]$ from t_i to the end of the inflation can be calculated by the standard formula given by Eq. (3.35).

- To be complete, in Section II we have also studied the evolution of the universe in which the total energy of the inflaton is dominated by the potential energy $V(\phi)$ at the quantum bounce, that is, $\frac{1}{2}\dot{\phi}^2(t_B) \ll V(\phi(t_B))$, and in particular, for the Starobinsky potential we have shown that slow-roll inflation never happens, which is consistent with the results obtained in [30, 31].

As noticed previously, the modified Friedmann equation (2.2) and the Klein-Gordon equation (2.3) are also derived in *the deformed algebra approach* [19–24]. So, all the results obtained for the evolution of the background in this paper are equally applicable to this approach. In fact, they are applicable to any theory of gravity in which the background is governed by Eqs.(2.2) and (2.3).

B. Perturbations and Observational Constraints

With the above understanding of the background evolution of the universe, we then turned to study the linear scalar and tensor perturbations during the above mentioned three different phases, and mainly found the following:

- During the bouncing and transition phases, the potential term $U(\phi)$ given by Eq. (4.7) for the scalar perturbations of Eq. (4.9) is always negligible in comparison with the term a''/a , as shown in Fig. 17. As a result, during these two phases, the scalar and tensor perturbations satisfy the same equation of motion, given by Eq. (4.11).
- During the bouncing phase, the effective potential $\mathcal{V}(\eta)[\equiv a''/a]$ given by Eq. (4.19) (for both scalar and tensor perturbations) can be well approximated by the PT potential (4.20), for which *an analytical expression for the mode functions $\mu_k^{(s,t)}$ exists, and is given by Eq. (4.26)*.

During the transition and slow-roll inflationary phases, the mode functions $\mu_k^{(s,t)}$ are also known analytically, and are given, respectively, by Eqs. (4.29) and (4.33).

- After matching the three solutions for the mode functions $\mu_k^{(s,t)}$ together, the coefficients α_k and β_k of the mode functions during the slow-roll inflationary phase are given by Eqs. (4.42) and (4.43) in

terms of a_k and b_k of the mode functions appearing in Eq. (4.26), which describe the pre-inflationary dynamics of the mode functions during the bouncing phase, and will be determined by the initial conditions. In general, it is expected that $\beta_k \neq 0$ at the onset of the slow-roll inflation, that is, *particles are generically created due to the pre-inflationary dynamics*. Note that in GR we normally impose the BD vacuum, $(\alpha_k^{\text{GR}}, \beta_k^{\text{GR}}) = (1, 0)$, at the onset of inflation [4].

- It is exactly because the particle creations during the pre-inflationary phases that *the Bogoliubov coefficients α_k and β_k in general depend on the wavenumber k via Eqs. (4.42), (4.43) and (4.25)*. It further implies that the power spectra, both scalar and tensor, will in general depend on k , that is, the power spectra are no longer scale-invariant, which provides a great opportunity to test the theory observationally. Such a dependence can be seen from Fig. 18, from which we can see that at the quantum bounce the modes with $k > k_B$ are all within the Hubble horizon, while the ones with $k < k_B$ are all outside the Hubble horizon. Depending on the ratio k/k_B , the modes have different dynamics during the pre-inflationary phases, although after the moment t_s all the modes will be inside the horizon. Certainly, this dependence cannot be very strong. Otherwise, it will be in conflict with current observations that show that the spectra are almost scale-invariant [6, 7].
- To determine a_k and b_k , we have considered two commonly used sets of initial conditions in Section V. One is the BD vacuum state imposed in the contracting phase [65], right prior to the bounce, as shown in Fig. 18. For $t < -t_s$, all the modes are within the Hubble horizon, so the BD vacuum state is a natural choice in this case. The other set is imposed at the bounce [38, 64]. As shown above, at this moment, some modes are inside the Hubble horizon, and some are outside of it. So, in this case the BD vacuum state is no longer a choice. Instead, we imposed *the fourth-order adiabatic vacuum state* [16–18]. Within the validity of the latter, however, we found that they essentially lead to the same results of the parameters a_k and b_k , all of which are given by Eq. (5.4).
- It is remarkable to note that the parameters a_k and b_k for both scalar and tensor perturbations are all given by Eq. (5.4). Then, the power spectra of the scalar and tensor perturbations are proportional to the same factor $|\alpha_k + \beta_k|^2$, as shown by Eqs. (4.48) and (4.52). As a result, *the ratio r between the tensor and scalar perturbations is the same as that given in GR*.
- In addition, after the effects of the pre-inflationary dynamics are taken into account, as shown above,

the power spectra now are generically scale-dependent. Therefore, by measuring the k -dependence of the power spectra, one can directly test LQC. Fitting the power spectra to the Planck 2015 temperature (TT+lowP) and polarization (TT,TE,EE+lowP) data, we found the total e-folds from the quantum bounce to the current time must be,

$$N_{\text{tot}} = \ln \left(\frac{a_0}{a_B} \right) > 141, \text{ (at 95\% C.L.)}, \quad (7.2)$$

that is, to be consistent with observations, the universe must have expanded at least 132 e-folds from the bounce until now, so the scale-dependent features are well diluted. Otherwise, it will be in conflict with current observations.

C. Outlook

With the above main results, we would like to note the following. The first issue is about the initial conditions of the perturbations. As we explained in Sec. V, this is a subtle issue during the bouncing phase because in general there is not a preferred initial state for a quantum field in arbitrarily curved spacetime [62, 66, 67] (see also [68, 69] for a recent discussion). The general solution of the Bogoliubov coefficients α_k and β_k given by Eqs. (4.42) and (4.43) are not limited to any specific set of the initial conditions. Instead, they are given in terms of the two parameters a_k and b_k , which are uniquely determined by initial conditions. So, in principle one can use these expressions to study the effects of the initial conditions. Recently, Ashtekar and Gupta [55, 68] have proposed other new initial states, some of which can explain the observed scalar spectrum suppression at large scales and thus fits the observations better than the standard power-law spectrum. It is also interesting to consider these initial conditions and its observational implications analytically, by using the formulas presented in this paper.

Since inflationary models with a single scalar field have been extensively studied in the framework of GR [4, 8], it would be very interesting to see if the effects of the pre-inflationary dynamics in other inflationary models could lead to any observational signatures, in addition to the ones found so far. In the standard inflationary models, one in general imposes the initial conditions for the background evolution simply by hand at the onset of the slow-roll inflation, while in LQC, as we discussed in Sec. II, the initial values of ϕ_B and $\dot{\phi}_B$ have to be chosen so that $H(t_B) = 0$ at the bounce, which imposes one additional constraint, so that only one degree of freedom for the scalar field is left. Moreover, as shown in Sec. VI, current observations already impose constraints on the total e-folds N_{tot} , so the k -dependent features are well diluted, in order to be consistent with current observations. Because the analytical formulas developed in this paper for

both background and perturbation evolutions are general, it would be very interesting to apply them to other inflationary models in order to see if further constraints can be obtained.

In addition, when we considered the Starobinsky potential, our analysis was limited to the Einstein frame. In the framework of GR, it was shown that they are equivalent. However, whether this is also true or not in LQC is still an open question. According to [72], in general the Einstein and Jordan frames are no longer equivalent at the quantum level. Thus, it is interesting to explore the Starobinsky model and its corresponding cosmological perturbations directly in the Jordan frame, based on the quantization proposed in [73, 74].

Yet, once particles are created, it is usually expected that non-Gaussianity will also raise [4, 8]. Therefore, it would be very interesting to study non-Gaussianity of primordial scalar and tensor perturbations by using the analytical solutions presented in this paper. Numerical studies were already carried out in [75].

We hope to return to the above issues soon in other occasions.

ACKNOWLEDGEMENTS

We would like to thank A. Barrau, S. Brahma, J. Lewandowski, A. Marciano and P. Singh for valuable comments and suggestions. Part of the work was reported in *the Informal Spring Meeting on Quantum Gravity, Shanghai 2017*, Fudan University, Shanghai, May 11-12, 2017, and *LOOPS' 17*, Warsaw, Poland, July 3 - 7, 2017. This work is supported in part by the Chinese NSF Grants, Nos. 11375153 (A.W.), 11675145 (A.W.), 11675143 (T.Z.), and 11105120 (T.Z.). K.K. was supported by the Baylor University Summer Sabbatical Programme.

Appendix A: Derivation of t_c for the Starobinsky potential

For the Starobinsky potential, the time t_c is determined by the equation

$$\frac{1}{2}\dot{\phi}_c^2 = \frac{3}{32\pi}M^2M_{\text{Pl}}^2 \left(1 - e^{-\sqrt{2/3}\phi_c/M_{\text{Pl}}} \right)^2, \quad (\text{A.1})$$

from which we find,

$$\pm\dot{\phi}_c = \sqrt{\frac{3}{16\pi}}Mm_{\text{Pl}} \left(1 - e^{-\sqrt{16\pi/3}\phi_c/m_{\text{Pl}}} \right). \quad (\text{A.2})$$

In the following we divide our discussions into two parts: $\dot{\phi}_c > 0$ and $\dot{\phi}_c < 0$.

1. $\dot{\phi}_c > 0$

In this case, we find

$$\dot{\phi}_c = \sqrt{\frac{3}{16\pi}} M m_{\text{Pl}} \left(1 - e^{-\sqrt{16\pi/3}\phi_c/m_{\text{Pl}}}\right), \quad (\text{A.3})$$

where we only consider the case $\phi_c > 0$, so the right-hand side of the above equation is always positive³, and ϕ_c and $\dot{\phi}_c$ are given, respectively, by

$$\phi_c \simeq \phi_B + \frac{m_{\text{Pl}}}{2\sqrt{3\pi}} \ln \left(2\sqrt{\gamma_B} \frac{t_c}{t_{\text{Pl}}}\right), \quad (\text{A.4})$$

$$\dot{\phi}_c \simeq \frac{m_{\text{Pl}}^2}{\sqrt{12\pi}} \frac{t_{\text{Pl}}}{t_c}. \quad (\text{A.5})$$

Since

$$\begin{aligned} & \exp\left(-\sqrt{\frac{16\pi}{3}} \frac{\phi_c}{m_{\text{Pl}}}\right) \\ &= 2^{-2/3} \left(\sqrt{\gamma_B} \frac{t_c}{t_{\text{Pl}}}\right)^{-2/3} e^{-\sqrt{16\pi/3}\phi_B/m_{\text{Pl}}}, \end{aligned} \quad (\text{A.6})$$

we have

$$\frac{m_{\text{Pl}}^2}{\sqrt{12\pi}} \frac{t_{\text{Pl}}}{t_c} = \sqrt{\frac{3}{16\pi}} M m_{\text{Pl}} \left[1 - 2^{-2/3} \left(\sqrt{\gamma_B} \frac{t_c}{t_{\text{Pl}}}\right)^{-2/3} e^{-\sqrt{16\pi/3}\phi_B/m_{\text{Pl}}}\right]. \quad (\text{A.7})$$

Solving this equation we obtain

$$t_c = \frac{2}{3M} + \frac{e^{-\frac{2\sqrt{3\pi}\phi_B}{m_{\text{Pl}}}} \left[\left(\sqrt{36\gamma_B m_{\text{Pl}}^2 e^{\frac{4\sqrt{3\pi}\phi_B}{m_{\text{Pl}}}} - 3M^2} + 6\sqrt{\gamma_B} m_{\text{Pl}} e^{\frac{2\sqrt{3\pi}\phi_B}{m_{\text{Pl}}}} \right)^{2/3} + (3M^2)^{1/3} \right]}{2(9M)^{1/3} \sqrt{\gamma_B} m_{\text{Pl}} \left(\sqrt{36\gamma_B m_{\text{Pl}}^2 e^{\frac{4\sqrt{3\pi}\phi_B}{m_{\text{Pl}}}} - 3M^2} + 6\sqrt{\gamma_B} m_{\text{Pl}} e^{\frac{2\sqrt{3\pi}\phi_B}{m_{\text{Pl}}}} \right)^{1/3}}. \quad (\text{A.8})$$

We can immediately see that, when ϕ_B becomes large, the above expression approaches

$$t_c \rightarrow \frac{2}{3M}, \quad (\text{A.9})$$

which implies that when the value of ϕ_B increases, t_c will approach a value that only depends on the parameter M .

2. $\dot{\phi}_c < 0$

In this case, we find

$$\dot{\phi}_c = -\sqrt{\frac{3}{16\pi}} M m_{\text{Pl}} \left(1 - e^{-\sqrt{16\pi/3}\phi_c/m_{\text{Pl}}}\right), \quad (\text{A.10})$$

where we also only consider the case $\phi_c > 0$, thus the right-hand side of the above equation is always negative and ϕ_c and $\dot{\phi}_c$ are given, respectively, by

$$\phi_c \simeq \phi_B - \frac{m_{\text{Pl}}}{2\sqrt{3\pi}} \ln \left(2\sqrt{\gamma_B} \frac{t_c}{t_{\text{Pl}}}\right), \quad (\text{A.11})$$

$$\dot{\phi}_c \simeq -\frac{m_{\text{Pl}}^2}{\sqrt{12\pi}} \frac{t_{\text{Pl}}}{t_c}. \quad (\text{A.12})$$

Since

$$\begin{aligned} & \exp\left(-\sqrt{\frac{16\pi}{3}} \frac{\phi_c}{m_{\text{Pl}}}\right) \\ &= 2^{2/3} \left(\sqrt{\gamma_B} \frac{t_c}{t_{\text{Pl}}}\right)^{2/3} e^{-\sqrt{16\pi/3}\phi_B/m_{\text{Pl}}}, \end{aligned} \quad (\text{A.13})$$

we have

$$\frac{m_{\text{Pl}}^2}{\sqrt{12\pi}} \frac{t_{\text{Pl}}}{t_c} = \sqrt{\frac{3}{16\pi}} M m_{\text{Pl}} \left[1 - 2^{2/3} \left(\sqrt{\gamma_B} \frac{t_c}{t_{\text{Pl}}}\right)^{2/3} e^{-\sqrt{16\pi/3}\phi_B/m_{\text{Pl}}}\right]. \quad (\text{A.14})$$

³ Even when we consider a negative value of ϕ_B as initial input, the scalar field will finally reach a positive value at $t = t_c$.

As we have shown numerically, in order to produce sufficient e-folds (≥ 60) during the slow-roll inflation, we have to require $\phi_B \in (3.61, +\infty)$. This leads to a simplification in the above equation, as the second terms in the square bracket can be neglected in comparison to the first term. Then, we find

$$t_c \simeq \frac{2}{3M}, \quad (\text{A.15})$$

which implies that when the value of ϕ_B increases, t_c will approach a value that only depends on the parameter M . In order to determine the weak dependence of t_c on ϕ_B , we can consider a small perturbation δt_c . Then, considering only the first-order expansion in terms of δt_c , we find

$$\delta t_c = \frac{2}{3M} \left(\frac{4\sqrt{\gamma_B} m_{\text{Pl}}}{3M} \right)^{2/3} e^{-\sqrt{16\pi/3}\phi_B/m_{\text{Pl}}}. \quad (\text{A.16})$$

Thus, finally we obtain

$$t_c = \frac{2}{3M} \left[1 + \left(\frac{4\sqrt{\gamma_B} m_{\text{Pl}}}{3M} \right)^{2/3} e^{-\sqrt{16\pi/3}\phi_B/m_{\text{Pl}}} \right]. \quad (\text{A.17})$$

Appendix B: Asymptotic expansion of $|\Gamma(x + iy)|$ for a large $|y|$

In this appendix we are going to derive the asymptotic behavior of the Gamma function $|\Gamma(x + iy)|$ when $|y|$ is large. Note that the following asymptotic formula of the $\Gamma(z)$ function at infinity (i.e., $|z| \rightarrow +\infty$) is known,

$$\Gamma(z) = \sqrt{2\pi} e^{-z} z^{z-1/2} \left(\sum_{k=0}^{\infty} \frac{g_k}{z^k} \right), \quad (\text{B.1})$$

where

$$\begin{aligned} g_0 &= 1, & g_1 &= \frac{1}{12}, & g_2 &= \frac{1}{288}, \\ g_3 &= -\frac{139}{51840}, & g_4 &= -\frac{571}{2488320}, & \dots & \end{aligned} \quad (\text{B.2})$$

Now we are going to use the above formula to calculate $\Gamma(x + iy)$. For this purpose, let us first consider the term e^{-z} with $z = x + iy$, which yields

$$e^{-z} = e^{-x} e^{-iy}. \quad (\text{B.3})$$

Turning to the term $z^{z-1/2}$, we have

$$(x + iy)^{x-1/2+iy}, \quad (\text{B.4})$$

and so we find,

$$(x - 1/2 + iy) \ln(x + iy)$$

$$\begin{aligned} &= (x - 1/2 + iy) \ln \left[\sqrt{x^2 + y^2} (\cos \theta + i \sin \theta) \right] \\ &= (x - 1/2 + iy) \left(\ln \sqrt{x^2 + y^2} + i\theta \right) \\ &= (x - 1/2) \ln \sqrt{x^2 + y^2} - \theta y \\ &\quad + i \left[\theta(x - 1/2) + y \ln \sqrt{x^2 + y^2} \right], \end{aligned} \quad (\text{B.5})$$

where $\theta \equiv \arccos \frac{x}{\sqrt{x^2 + y^2}}$. Thus, we finally get

$$\begin{aligned} z^{z-1/2} &= (x^2 + y^2)^{\frac{1}{2}(x-\frac{1}{2})} e^{-\theta y} \\ &\quad \times e^{i \left[\theta(x-1/2) + y \ln \sqrt{x^2 + y^2} \right]}. \end{aligned} \quad (\text{B.6})$$

We need to expand the above expression about $y \rightarrow \infty$ up to the fourth-order. First, for $(x^2 + y^2)^{\frac{x}{2} - \frac{1}{4}}$, we find

$$\begin{aligned} &(x^2 + y^2)^{\frac{x}{2} - \frac{1}{4}} \\ &= y^{x-\frac{1}{2}} \left(1 + \frac{x^2}{y^2} \right)^{\frac{x}{2} - \frac{1}{4}} \\ &= y^{x-\frac{1}{2}} \left[1 + \left(\frac{x^3}{2} - \frac{x^2}{4} \right) \frac{1}{y^2} \right. \\ &\quad \left. + \left(\frac{5x^4}{32} - \frac{3x^5}{8} + \frac{x^6}{8} \right) \frac{1}{y^4} + \mathcal{O} \left(\frac{1}{y^4} \right) \right]. \end{aligned} \quad (\text{B.7})$$

Considering $e^{-\theta y}$, first we have

$$\begin{aligned} \theta &= \arccos \left(\frac{x}{\sqrt{x^2 + y^2}} \right) \\ &= \arccos \left(\frac{x}{y} \frac{1}{\sqrt{1 + \frac{x^2}{y^2}}} \right) \\ &= \frac{\pi}{2} - \frac{x}{y} + \frac{x^3}{3} \frac{1}{y^3} - \frac{x^5}{5} \frac{1}{y^5} + \mathcal{O} \left(\frac{1}{y^7} \right), \end{aligned} \quad (\text{B.8})$$

thus, we get

$$-\theta y = -\frac{\pi y}{2} + x - \frac{x^3}{3} \frac{1}{y^2} + \frac{x^5}{5} \frac{1}{y^4} + \mathcal{O} \left(\frac{1}{y^6} \right), \quad (\text{B.9})$$

and

$$\begin{aligned} e^{-\theta y} &= e^{-\frac{\pi y}{2} + x} e^{-\frac{x^3}{3} \frac{1}{y^2}} \\ &\simeq e^{-\frac{\pi y}{2} + x} \left[1 - \frac{x^3}{3} \frac{1}{y^2} + \left(\frac{x^5}{5} + \frac{x^6}{18} \right) \frac{1}{y^4} \right]. \end{aligned} \quad (\text{B.10})$$

For the terms in the bracket of Eq. (B.1), if we only consider the first four terms in the expansion⁴, we have

$$\begin{aligned}
\left(\sum_{k=0}^{\infty} \frac{g_k}{z^k}\right) &= g_0 + \frac{g_1}{z} + \frac{g_2}{z^2} + \frac{g_3}{z^3} + \frac{g_4}{z^4} + \mathcal{O}\left(\frac{1}{z^5}\right) \\
&= \left[g_0^2 + \frac{g_1^2 - 2g_0g_2 + 2g_0g_1x}{x^2 + y^2} + \frac{g_2^2 - 2g_1g_3 + 2g_0g_4 + 2(g_1g_2 - 3g_0g_3)x + 4g_0g_2x^2}{(x^2 + y^2)^2} \right. \\
&\quad + \frac{g_3^2 - 2g_2g_4 + 2(g_2g_3 - 3g_1g_4)x + 4(g_1g_3 - 4g_0g_4)x^2 + 8g_0g_3x^3}{(x^2 + y^2)^3} \\
&\quad \left. + \frac{g_4^2 + 2g_3g_4x + 4g_2g_4x^2 + 8g_1g_4x^3 + 16g_0g_4x^4}{(x^2 + y^2)^4} \right]^{1/2} e^{i\vartheta} \tag{B.11}
\end{aligned}$$

$$\begin{aligned}
&\simeq \left\{ g_0 + \left(\frac{g_1^2}{2g_0} - g_2 + g_1x \right) \frac{1}{y^2} \right. \\
&\quad \left. + \left[g_1x^3 + \left(\frac{g_1^2}{g_0} - 3g_2 \right) x^2 + \left(\frac{g_1^3}{2g_0^2} - \frac{2g_1g_2}{g_0} + 3g_3 \right) x + \frac{g_1^4}{8g_0^3} - \frac{g_1^2g_2}{2g_0^2} + \frac{g_1g_3}{g_0} - g_4 \right] \frac{1}{y^4} + \mathcal{O}\left(\frac{1}{y^6}\right) \right\} e^{i\vartheta}. \tag{B.12}
\end{aligned}$$

Finally, combining all the above expansions together, we find

$$|\Gamma(x + iy)| = \sqrt{2\pi} |y|^{x-\frac{1}{2}} e^{-\frac{\pi y}{2}} \left[1 + \left(\frac{x^3}{6} - \frac{x^2}{4} + \frac{x}{12} \right) \frac{1}{y^2} + \left(\frac{x^6}{72} - \frac{11x^5}{120} + \frac{49x^4}{288} - \frac{5x^3}{48} + \frac{x^2}{288} + \frac{x}{120} \right) \frac{1}{y^4} + \mathcal{O}\left(\frac{1}{y^6}\right) \right]. \tag{B.13}$$

-
- [1] A. H. Guth, Inflationary universe: A possible solution to the horizon and flatness problems, *Phys. Rev. D* **23**, 347 (1981).
- [2] K. Sato, First-order phase transition of a vacuum and the expansion of the Universe *Monthly Notices of the Royal Astronomical Society* **195**, 467 (1981).
- [3] A. A. Starobinsky, A new type of isotropic cosmological models without singularity, *Phys. Lett. B* **91**, 99 (1980).
- [4] D. Baumann, TASI Lectures on Inflation, [arXiv:0907.5424](https://arxiv.org/abs/0907.5424); D. Baumann and L. McAllister, *Inflation and String Theory* (Cambridge Monographs on Mathematical Physics, Cambridge University Press, 2015); E. Silverstein, *TASI lectures on cosmological observables and string theory*, [arXiv:1606.03640](https://arxiv.org/abs/1606.03640).
- [5] E. Komatsu *et al.*, Seven-year Wilkinson Microwave Anisotropy Probe (WMAP) Observations: Cosmological Interpretation, *ApJS* **192**, 18 (2011).
- [6] Planck Collaboration *et al.*, Planck 2013 results. XXII. Constraints on inflation, *Astronomy & Astrophysics* **571**, A22 (2014).
- [7] P. Collaboration *et al.*, Planck 2015. XX. Constraints on inflation, [arXiv:1502.02114](https://arxiv.org/abs/1502.02114) [astro-ph].
- [8] J. Martin, C. Ringeval, and V. Vennin, *Encyclopaedia Inflationaris*, *Phys. Dark Univ.* **5** (2014) 75 [[arXiv:1303.3787](https://arxiv.org/abs/1303.3787)].
- [9] J. Martin and R. H. Brandenberger, Trans-Planckian problem of inflationary cosmology, *Phys. Rev. D* **63**, 123501 (2001).
- [10] R. H. Brandenberger and J. Martin, Trans-Planckian issues for inflationary cosmology, *Class. Quantum Grav.* **30**, 113001 (2013).
- [11] A. Borde and A. Vilenkin, Eternal inflation and the initial singularity, *Phys. Rev. Lett.* **72**, 3305 (1994).
- [12] A. Borde, A. H. Guth, and A. Vilenkin, Inflationary Spacetimes Are Incomplete in Past Directions, *Phys. Rev. Lett.* **90**, 151301 (2003).
- [13] A. Ashtekar and P. Singh, *Loop quantum cosmology: a status report*, *Class. Quantum Grav.* **28**, 213001 (2011); I. Agullo and P. Singh, Loop Quantum Cosmology: A brief review, [arXiv:1612.01236](https://arxiv.org/abs/1612.01236).
- [14] M. Bojowald, Quantum cosmology: a review, *Rep. Prog. Phys.* **78** (2015) 023901 [[arXiv:1501.04899](https://arxiv.org/abs/1501.04899)].
- [15] A. Ashtekar, W. Kaminski, and J. Lewandowski, Quantum field theory on a cosmological, quantum space-time, *Phys. Rev. D* **79** (2009) 064030.
- [16] I. Agullo, A. Ashtekar, and W. Nelson, Quantum Gravity Extension of the Inflationary Scenario, *Phys. Rev. Lett.* **109**, 251301 (2012).
- [17] I. Agullo, A. Ashtekar, and W. Nelson, Extension of the quantum theory of cosmological perturbations to the Planck era, *Phys. Rev. D* **87**, 043507 (2013).
- [18] I. Agullo, A. Ashtekar, and W. Nelson, The pre-

⁴ The fifth or higher terms only contribute to the order $\mathcal{O}(1/y^6)$ in the expansion.

- inflationary dynamics of loop quantum cosmology: confronting quantum gravity with observations, *Class. Quantum Grav.* **30**, 085014 (2013).
- [19] M. Bojowald, G. M. Hossain, M. Kagan, and S. Shankaranarayanan, Gauge invariant cosmological perturbation equations with corrections from loop quantum gravity, *Phys. Rev. D* **79**, 043505 (2009).
- [20] J. Mielczarek, T. Cailleteau, A. Barrau, and J. Grain, Anomaly-free vector perturbations with holonomy corrections in loop quantum cosmology, *Class. Quant. Grav.* **29**, 085009 (2012) [arXiv:1106.3744].
- [21] T. Cailleteau, J. Mielczarek, A. Barrau, and J. Grain, Anomaly-free scalar perturbations with holonomy corrections in loop quantum cosmology, *Class. Quant. Grav.* **29**, 095010 (2012) [arXiv:1111.3535].
- [22] T. Cailleteau, A. Barrau, J. Grain and F. Vidotto, Consistency of holonomy-corrected scalar, vector and tensor perturbations in Loop Quantum Cosmology, *Phys. Rev. D* **86**, 087301 (2012) [arXiv:1206.6736].
- [23] T. Cailleteau, L. Linsefors, and A. Barrau, Anomaly-free perturbations with inverse-volume and holonomy corrections in loop quantum cosmology, *Class. Quantum Grav.* **31**, 125011 (2014) [arXiv:1307.5238].
- [24] A. Barrau, M. Bojowald, G. Calcagni, J. Grain, and M. Khagan, Anomaly-free cosmological perturbations in effective canonical quantum gravity, *J. Cosmol. Astropart. Phys.* **05** (2015) 051 [arXiv:1404.1018].
- [25] M. Bojowald, G. Calcagni, and S. Tsujikawa, Observational Constraints on Loop Quantum Cosmology, *Phys. Rev. Lett.* **107**, 211302 (2011) [arXiv:1101.5391].
- [26] M. Bojowald, G. Calcagni, and S. Tsujikawa, Observational test of inflation in loop quantum cosmology, *J. Cosmol. Astropart. Phys.* **11** (2011) 046 [arXiv:1107.1540].
- [27] T. Zhu, A. Wang, G. Cleaver, K. Kirsten, Q. Sheng, and Q. Wu, Detecting quantum gravitational effects of loop quantum cosmology in the early universe?, *Astrophys. J. Lett.* **807** (2015) L17 [arXiv:1503.06761].
- [28] T. Zhu, A. Wang, G. Cleaver, K. Kirsten, Q. Sheng, and Q. Wu, Scalar and tensor perturbations in loop quantum cosmology: High-order corrections, *J. Cosmol. Astropart. Phys.* **10** (2015) 052 [arXiv:1508.03239].
- [29] T. Zhu, A. Wang, G. Cleaver, K. Kirsten, Q. Sheng, and Q. Wu, Inflationary spectra with inverse-volume corrections in loop quantum cosmology and their observational constraints from Planck 2015 data, *J. Cosmol. Astropart. Phys.* **03** (2016) 046 [arXiv:1510.03855].
- [30] B. Bonga and B. Gupta, Inflation with the Starobinsky potential in loop quantum cosmology, *Gen Relativ Gravit* **48**, 1 (2016).
- [31] B. Bonga and B. Gupta, Phenomenological investigation of a quantum gravity extension of inflation with the Starobinsky potential, *Phys. Rev. D* **93**, 063513 (2016).
- [32] M. Bojowald, Absence of a Singularity in Loop Quantum Cosmology, *Phys. Rev. Lett.* **86**, 5227 (2001).
- [33] A. Ashtekar, T. Pawłowski, and P. Singh, Quantum Nature of the Big Bang, *Phys. Rev. Lett.* **96**, 141301 (2006).
- [34] A. Ashtekar, T. Pawłowski, and P. Singh, Quantum nature of the big bang: An analytical and numerical investigation, *Phys. Rev. D* **73**, 124038 (2006).
- [35] A. Ashtekar, T. Pawłowski, and P. Singh, Quantum nature of the big bang: Improved dynamics, *Phys. Rev. D* **74**, 084003 (2006).
- [36] A. Ashtekar, A. Corichi, and P. Singh, Robustness of key features of loop quantum cosmology, *Phys. Rev. D* **77**, 024046 (2008).
- [37] J. Yang, Y. Ding, and Y. Ma, Alternative quantization of the Hamiltonian in loop quantum cosmology, *Phys. Lett. B* **682**, 1 (2009).
- [38] A. Ashtekar and D. Sloan, Loop quantum cosmology and slow roll inflation, *Phys. Lett. B* **694**, 108 (2010).
- [39] A. Ashtekar and D. Sloan, Probability of inflation in loop quantum cosmology, *Gen Relativ Gravit* **43**, 3619 (2011).
- [40] P. Singh, K. Vandersloot, and G. V. Vereshchagin, Non-singular bouncing universes in loop quantum cosmology, *Phys. Rev. D* **74**, 043510 (2006).
- [41] J. Mielczarek, T. Cailleteau, J. Grain, and A. Barrau, Inflation in loop quantum cosmology: Dynamics and spectrum of gravitational waves, *Phys. Rev. D* **81**, 104049 (2010).
- [42] X. Zhang and Y. Ling, Inflationary universe in loop quantum cosmology, *J. Cosmol. Astropart. Phys.* **08**, 012 (2007).
- [43] L. Chen and J.-Y. Zhu, Loop quantum cosmology: the horizon problem and the probability of inflation, *Phys. Rev. D* **92**, 084063 (2015) [arXiv:1510.03135 [gr-qc]].
- [44] B. Bolliet, J. Grain, C. Stahl, L. Linsefors, and A. Barrau, Comparison of primordial tensor power spectra from the deformed algebra and dressed metric approaches in loop quantum cosmology, *Phys. Rev. D* **91**, 084035 (2015).
- [45] S. Schander *et al.*, Primordial scalar power spectrum from the Euclidean big bounce, *Phys. Rev. D* **93**, 023531 (2016).
- [46] I. Agullo and O. Singh, Loop Quantum Cosmology: A brief review, arXiv:1612.01236[gr-qc].
- [47] P. Singh (editor), *Inter. J. Mod. Phys. D* **25**, No. 8, Special Issue on *Loop Quantum Cosmology*, 2016.
- [48] A. Ashtekar and J. Pullin (editors), *Loop Quantum Gravity: The First 30 Years* (Wold Scientific, 2017).
- [49] A. Barrau and B. Bolliet, Some conceptual issues in loop quantum cosmology, *Int. J. Mod. Phys. D* **25**, 1642008 (2016).
- [50] E. Wilson-Ewing, Separate universes in loop quantum cosmology: Framework and application, *Inter. J. Mod. Phys. D* **25**, 1642002 (2016), and references therein.
- [51] B.E. Navascures, M. Martin-Benito, and G.A.M. Marugan, Hybrid models in loop quantum cosmology, *Inter. J. Mod. Phys. D* **25**, 1642007 (2016), and references therein.
- [52] D.A. Graig, The consistent histories approach to loop quantum cosmology, *Inter. J. Mod. Phys. D* **25**, 1642009 (2016), and references therein.
- [53] B. Bolliet, A. Barrau, J. Grain, and S. Schander, Observational exclusion of a consistent loop quantum cosmology scenario, *Phys. Rev. D* **93**, 124011 (2016).
- [54] J. Grain, The perturbed universe in the deformed algebra approach of loop quantum cosmology, *Inter. J. Mod. Phys. D* **25**, 1642003 (2016).
- [55] A. Ashtekar and B. Gupta, Quantum gravity in the sky: interplay between fundamental theory and observations, *Class. Quantum Grav.* **34**, 014002 (2017).
- [56] I. Agullo and N. A. Morris, Detailed analysis of the predictions of loop quantum cosmology for the primordial power spectra, *Phys. Rev. D* **92**, 124040 (2015).
- [57] T. Zhu, A. Wang, K. Kirsten, G. Cleaver, and Q. Sheng, Universal features of quantum bounce in loop quantum cosmology, arXiv:1607.06329.
- [58] V. Taveras, Corrections to the Friedmann equations from

- loop quantum gravity for a universe with a free scalar field, *Phys. Rev. D* **78**, 064072 (2008).
- [59] M. Bojowald and A. Skirzewski, Effective equations of motion for quantum systems, *Rev. Math. Phys.* **18**, 713 (2006).
- [60] M. Bojowald, B. Sandhofer, A. Skirzewski, and A. Tsobanian, Effective constraints for quantum systems, *Rev. Math. Phys.* **21**, 111 (2009).
- [61] J. Mielczarek, M. Kamionka, A. Kurek, and M. Szydlowski, Observational hints on the Big Bounce, *J. Cosmol. Astropart. Phys.* **2010**, 004 (2010).
- [62] S. Winitzki, Cosmological particle production and the precision of the WKB approximation, *Phys. Rev. D* **72**, 104011 (2005).
- [63] C. Germani, W. Nelson, and M. Sakellariadou, Onset of inflation in loop quantum cosmology, *Phys. Rev. D* **76**, 043529 (2007).
- [64] A. Corichi and A. Karami, On the measure problem in slow roll inflation and loop quantum cosmology, *Phys. Rev. D* **83**, 104006 (2011).
- [65] L. Linsefors and A. Barrau, Duration of inflation and conditions at the bounce as a prediction of effective isotropic loop quantum cosmology, *Phys. Rev. D* **87**, 123509 (2013).
- [66] I. Agullo and A. Ashtekar, Unitarity and ultraviolet regularity in cosmology, *Phys. Rev. D* **91**, 124010 (2015).
- [67] I. Agullo, W. Nelson, and A. Ashtekar, Preferred instantaneous vacuum for linear scalar fields in cosmological space-times, *Phys. Rev. D* **91**, 064051 (2015).
- [68] A. Ashtekar and B. Gupt, Initial conditions for cosmological perturbations, *Class. Quantum Grav.* **34**, 035004 (2017).
- [69] K. Martineau, A. Barrau, and S. Schander, Detailed investigation of the duration of inflation in loop quantum cosmology for a Bianchi I universe with different inflaton potentials and initial conditions, *Phys. Rev. D* **95** (2017) 083507.
- [70] A. Lewis and S. Bridle, Cosmological parameters from CMB and other data: A Monte Carlo approach, *Phys. Rev. D* **66**, 103511 (2002).
- [71] P. Collaboration *et al.*, Planck 2013 results. XVI. Cosmological parameters, [arXiv:1303.5076](https://arxiv.org/abs/1303.5076).
- [72] M. Artymowski, Y. Ma, and X. Zhang, Comparison between Jordan and Einstein frames of Brans-Dicke gravity a la loop quantum cosmology, *Phys. Rev. D* **88**, 104010 (2013).
- [73] X. Zhang and Y. Ma, Extension of Loop Quantum Gravity to f(R) Theories, *Phys. Rev. Lett.* **106**, 171301 (2011).
- [74] X. Zhang, M. Artymowski, and Y. Ma, Loop quantum Brans-Dicke cosmology, *Phys. Rev. D* **87**, 084024 (2013).
- [75] I. Agullo, Loop quantum cosmology, non-Gaussianity, and CMB power asymmetry, *Phys. Rev. D* **92**, 064038 (2015).